Astron. Astrophys. 344, 817–847 (1999)

ASTRONOMY AND ASTROPHYSICS

Molecular abundance variations in the Magellanic Clouds⋆,⋆⋆

A. Heikkilä[1,⋆⋆⋆], **L.E.B. Johansson**[1], **and H. Olofsson**[2]

[1] Onsala Space Observatory, S-439 92 Onsala, Sweden
[2] Stockholm Observatory, S-133 36 Saltsjöbaden, Sweden

Received 15 July 1998 / Accepted 10 December 1998

Abstract. We have observationally studied the effect of metallicity and far-ultraviolet (FUV) radiation on the physical conditions and the molecular abundances in interstellar clouds in the Small and the Large Magellanic Clouds (SMC and LMC, respectively). Spectral line emission from a number of molecules was observed in a sequence of clouds with positions in and between the 30 Doradus (30Dor) and the southern part of the N159 region in the LMC, and in one cloud (N27, also denoted LIRS 49) located in the SMC bar. Physical conditions and molecular abundances were estimated from the observational data by excitation and radiative transfer calculations. A comparison of the molecular abundances in clouds in the SMC, the LMC, and the Galaxy is presented. We also report the first detection of hydrogen sulphide (ortho-H_2S) in an extragalactic source, detections of methanol (CH_3OH) in thermal emission and methyl acetylene (CH_3CCH), and a tentative detection of thio-formaldehyde (H_2CS) in N159W.

The abundances (relative to H_2) of molecular species (except CO) in the LMC sources and in N27 are estimated to be typically 5×10^{-10}, and 1×10^{-10}, respectively. These values apply to the gas volume defined by the CO line emission. Relative to Galactic clouds, the abundances in N159W (our reference cloud) are five to twenty times lower. In two of the clouds: N27 and the centremost cloud in 30Dor (30Dor-10), the derived abundances deviate significantly from those in the other clouds in our sample, by being on the average six and eight times lower, respectively. In N27, the most likely explanation is the lower metallicity in the SMC, whereas the underabundance in 30Dor-10 is probably mainly caused by a more rapid photodissociation due to the more intense FUV radiation in this area. An alternative explanation for the underabundances in both N27 and 30Dor-10 would be a higher H/H_2 ratio inside these molecular clouds. The ethynyl radical (C_2H), with an estimated average abundance of 5×10^{-9} in seven clouds in the LMC and 3×10^{-9} in two clouds in the SMC, is the most abundant observed trace molecule after the CO isotopomers. Qualitatively, the high C_2H abundance can be explained as reflecting the C^+-rich and FUV photon-rich environment, i.e., a chemistry characteristic for photon-dominated regions.

For N27 we have, using HCO^+ and $H^{13}CO^+$ data, estimated the gas-phase $^{12}C/^{13}C$ ratio to be 40–90, a range that encompasses the values found in N159W and in Galactic disc clouds.

In all clouds in our sample, the number density estimates from an excitation analysis of CS, SO, HCO^+, HCN and H_2CO are in the range (1–100)$\times10^4$ cm^{-3}. CO data gives a lower limit of a few$\times10^3$ cm^{-3}. However, the average densities (estimated from the virial mass) are significantly lower, typically a few$\times10^2$ cm^{-3}, suggesting that the clouds (as probed by trace molecules) are very clumpy with volume-filling factors $\ll$1. In N159W, where our data-base is by far most extensive, the number density and the kinetic temperature of molecular hydrogen in the dense part of the gas are estimated to be (1–10)$\times10^5$ cm^{-3} and 25$\pm$10 K, respectively. The corresponding numbers in N27 are, although based on less data than in N159W, (5–50)$\times10^4$ cm^{-3} and 15$\pm$5 K. Thus, the metallicity difference between the LMC and the SMC does not seem to affect the density and the temperature of the gas dramatically.

In the SMC, the CO(J=1–0)/HCO^+(J=1–0) line intensity ratio follows the same trend with respect to the star-formation activity as in the LMC: a lower ratio is found in clouds with a more vigorous star-formation activity. A similar trend is also exhibited by the CO(J=1–0)/C_2H(N=1–0) line intensity ratio in the LMC.

Key words: ISM: molecules – galaxies: abundances – galaxies: ISM – galaxies: Magellanic Clouds – radio lines: galaxies – radio lines: ISM

1. Introduction

The global properties of the Small and Large Magellanic Clouds (SMC and LMC, respectively), two nearby irregular galaxies, differ considerably from those of the Milky Way Galaxy. Distinct features of the LMC and the SMC are their low heavy-element contents (metallicities), low dust-to-gas ratios, high

Send offprint requests to: A. Heikkilä

⋆ Based on observations using the Swedish-ESO Submillimetre Telescope (SEST) at the European Southern Observatory (ESO), La Silla, Chile.

⋆⋆ Figs. 3–14 are only available in the electronic version of this paper.

⋆⋆⋆ *Present address:* Observatory, P.O. Box 14, FIN-000 14 University of Helsinki, Finland

oxygen-to-carbon (O/C) ratios in H II regions, high atomic-to-molecular hydrogen (H/H_2) ratios, and intense radiation at ultraviolet (UV) and far-ultraviolet (FUV) wavelengths (see e.g. Westerlund 1990, 1997). The metallicity and the dust-to-gas ratio decrease, while the intensity of the radiation, the O/C ratio and the H/H_2 ratio increase, in the sequence the Galaxy-the LMC-the SMC. The high gas-to-total mass ratio and the deficit of heavy-elements and dust are considered to indicate that the Magellanic Clouds are chemically less evolved systems than the Galaxy. On the other hand, the intense radiation in the UV and FUV reflects the vigorous star-formation activity that is present in some parts of the LMC and the SMC. Such an activity is possibly induced by large-scale gravitational and/or hydrodynamic interactions between the Galaxy and the LMC and the SMC (see e.g. Westerlund 1990, 1997). Whether the star-formation histories of the Magellanic Clouds have been dominated by bursts or have been a more smooth process is still under debate; e.g. Feast (1995), Holtzman et al. (1997) and Stappers et al. (1997) have argued for a relatively constant star-formation rate, with a slight increase a few billion years ago.

The star-formation history and the compositions of stellar generations, the present as well as past ones, are closely coupled to the nature of the interstellar medium (ISM). In particular, the molecular component of the ISM is important since it contains the main birth-sites of stars. The Magellanic Clouds are excellent targets for studying the role of the environment in the formation and the evolution of molecular clouds and stars. Moreover, being low-metallicity objects, the Magellanic Clouds, in particular the SMC, may be useful test-objects for the conditions in systems in the Early Universe. Also, the proximity of the LMC and the SMC enables individual molecular clouds to be resolved even with single-dish telescopes. Accordingly, in the Magellanic Clouds, the gas properties can be studied in much more detail than in other more distant extragalactic objects.

A number of studies of the molecular ISM in the Magellanic Clouds using emission lines from the carbon monoxide (CO) molecule have been reported, beginning with the pioneering works of Huggins et al. (1975) and Israel et al. (1982, 1986). Cohen et al. (1988) and Rubio et al. (1991) presented large-scale surveys made with the 1.2m Columbia telescope located at Cerro Tololo, Chile. More recent CO studies are the spatially more detailed observations with the 15m Swedish-ESO Submillimetre Telescope (SEST) at La Silla, Chile, see Rubio et al. (1996), Johansson et al. (1998), and references therein. However, investigations involving other molecules are still relatively scarce, although the data-base of observed molecular spectral lines in the LMC and the SMC is growing rapidly. Therefore, the physical and the chemical properties of the molecular ISM in the Magellanic Clouds are still poorly known. Johansson (1991) summarised the first results of molecular line surveys in the LMC and the SMC conducted with the SEST in the late 1980's. Johansson et al. (1994) (hereafter Paper I) presented results of a line-survey in the λ=3 and 1.3 mm wavelength bands towards the position with the strongest CO(J=1–0) line intensity in the N159 region in the LMC (in the present work denoted N159W). The fractional abundances of molecules were estimated to be about ten times lower than those in Galactic disc clouds. The $^{12}C/^{13}C$ abundance ratio was estimated and the $^{32}S/^{34}S$ abundance ratio was assumed to be similar to those in Galactic disc clouds, while the $^{18}O/^{17}O$ abundance ratio showed a remarkably low value of 2. Recently, we estimated the $^{18}O/^{17}O$ ratio in four molecular clouds in the LMC and obtained an average of 1.6 (Heikkilä et al. 1998). Lequeux et al. (1994) published model calculations concerning the physical state of molecular clouds in the SMC. Their calculations were based solely on ^{12}CO and ^{13}CO data, and could therefore not describe the denser part of the gas. Chin et al. (1997) presented observations of molecular line emission in the λ=3 mm band in several clouds in the LMC and in one cloud (LIRS 36) in the SMC. Moreover, Chin et al. (1998) published a larger data-base of molecular line emission in LIRS 36, including data in the λ=3, 2, 1.3, and 0.8 mm wavelength bands, and estimated molecular abundances and physical conditions. The first detections of deuterated molecules (DCO^+ and DCN) in an external galaxy (LMC) were reported by Chin et al. (1996b) and Heikkilä et al. (1997a).

Table 1. Source coordinates

Cloud	$\alpha(1950.0)$	$\delta(1950.0)$
N159W	$05^h40^m03.0^s$	$-69°47'03''$
N159S	$05^h40^m27.1^s$	$-69°52'00''$
N160	$05^h40^m06.2^s$	$-69°40'28''$
30Dor-10	$05^h39^m11.4^s$	$-69°05'59''$
30Dor-27	$05^h36^m10.4^s$	$-69°14'31''$
N27	$00^h46^m32.9^s$	$-73°21'50''$

In this paper we enlarge the existing data-base of observed molecular line emission in the Magellanic Clouds, and study the effects of the low metallicity and the intense FUV radiation on the characteristics of their molecular ISM. To extend the study of the effect of the metallicity, we observed line emission from various molecules in the molecular gas cloud associated with the H II region N27 in the SMC. The effect of varying exposure to FUV radiation was further investigated by observations of line emission from a number of molecules in a sample of clouds in the LMC. The chosen LMC clouds are all located in the 30 Doradus (30Dor) area and the chain of H II regions (N158, N160, N159) south of it. From the observational data, we estimated the physical conditions and the molecular abundances in these clouds. Preliminary results of this work have been reported by Heikkilä (1996), Heikkilä et al. (1997b), and Johansson (1997).

2. Description of the sources

Below follows short descriptions of the observed regions. A more extensive summary of the 30Dor and N159 areas can be found in Johansson et al. (1998). The source coordinates are given in Table 1. For references to line emission maps of CO and other molecules, see Sect. 4.1. The dust temperature estimates quoted below are based on the 100/60 μm flux ratio taken from Schwering (1988). The quoted FUV fluxes (in the range 6 eV–13.6 eV) were calculated using data from Poglitsch et al. (1995) and Israel et al. (1996). The given Hα fluxes are taken from

Caplan & Deharveng (1985, 1986) and Caplan et al. (1996). In most cases the Hα observations refer to a significantly larger area (about 5′) than the extent of the associated molecular clouds (about 1′). Nevertheless, these Hα fluxes can be of interest in the description of the radiation environment of the molecular clouds.

2.1. N27 in the SMC

N27 is a bright and relatively compact H II region located in the south-western bar of the SMC. It is associated with the IRAS point source LIRS 49 (Schwering & Israel 1989). The velocity-integrated CO(J=1–0, 2–1 and 3–2) line intensities of the molecular cloud associated with N27 are the highest observed in the SMC. The Hα flux and the dust temperature are $0.15\times10^{-10}\,\mathrm{erg\,s^{-1}\,cm^{-2}}$ and 35–40 K, respectively. Caldwell (1997) estimated a dust temperature of 33–40 K for this cloud.

2.2. 30Dor area in the LMC

30Dor is the most spectacular star-forming region in the Local Group. The ISM in this area is exposed to a very violent environment composed of intense radiation and stellar winds emerging from clusters of massive stars. The molecular cloud associated with the centre of the 30Dor nebula is denoted 30Dor-10 (Johansson et al. 1998). The location indicates that this cloud is exposed to the most extreme environment in our sample. This is e.g. reflected in the line profiles, which are considerably broader ($\approx$10–15 km s^{-1}) than in other clouds ($\approx$5–8 km s^{-1}). Moreover, the CO(J=1–0) brightness temperature is lower ($\approx$1.5 K), suggesting a higher degree of clumping, and/or lower molecular abundances, compared to other clouds. The most likely explanation is low molecular abundances (cf. Sects. 5.2.3 and 5.2.5). The FUV flux, the Hα flux and the dust temperature in the central part of the 30Dor nebula are $9.4\,\mathrm{erg\,s^{-1}\,cm^{-2}}$, $41\times10^{-10}\,\mathrm{erg\,s^{-1}\,cm^{-2}}$ and 70 K, respectively. Werner et al. (1978) estimated a dust temperature of 75 K in 30Dor.

30Dor-27 is a cloud located at the outer edge of the 30Dor nebula (Johansson et al. 1998). The projected distance to the centre of 30Dor is 240 pc and should lead to a considerable dilution of the FUV radiation from the central part of the nebula. Thus, the radiation environment of this cloud is probably dominated by local H II regions and consequently less extreme than that of 30Dor-10. The Hα flux and the dust temperature are $3.1\times10^{-10}\,\mathrm{erg\,s^{-1}\,cm^{-2}}$ and 30–40 K, respectively.

2.3. N159 and N160 regions in the LMC

The N159 area contains several H II regions. The CO line emission shows three peaks: N159W, N159E, and N159S, from which we have chosen to study N159W and N159S due to their apparently different nature. N159E and N159W show similar properties (Paper I). N159W is associated with a prominent star-formation region and has the highest observed CO(J=1–0, 2–1, and 3–2) velocity-integrated line intensities in the LMC. N159S, on the contrary, lacks signs of on-going star-formation activity and appears to be a cold, more quiescent cloud. It is located at a projected distance of 90 pc south of N159W; the illumination by the stellar clusters in the N159W area is thus significantly diluted. The bright H II region N160 is located in between 30Dor and N159. The CO line emission associated with this nebula is complex with overlapping velocity components. We have chosen the position of the strongest feature, denoted N160-4 in Johansson et al. (1998). The FUV flux is 0.40–0.96 $\mathrm{erg\,s^{-1}\,cm^{-2}}$ in N159W, 0.016–0.11 $\mathrm{erg\,s^{-1}\,cm^{-2}}$ in N159S, and 0.32–0.72 $\mathrm{erg\,s^{-1}\,cm^{-2}}$ in N160. The Hα flux is $6.2\times10^{-10}\,\mathrm{erg\,s^{-1}\,cm^{-2}}$ near the N159W area and $6.0\times10^{-10}\,\mathrm{erg\,s^{-1}\,cm^{-2}}$ in N160. The dust temperature is 30–40 K in both N159W and N160, while 100/60 μm data are lacking for N159S.

3. Observations

The observations were carried out in February, June and December 1995, August and December 1996, February 1997, and June 1998 using the SEST[1] at La Silla, Chile. The receiver system used in February 1995 was a 3mm Schottky mixer and a 1.3mm SIS mixer. The 3mm receiver was replaced in May 1995 with a cryogenic SIS receiver. At the same time a 2mm SIS receiver was taken into operation. In November 1996 a new 1.3mm SIS mixer was installed. CO(J=3–2) observations were made with the 0.8mm SIS mixer in June 1995 and August 1996. All observations were made with the receivers tuned to single-sideband mode and connected to a high-resolution (2000 channels with a total bandwidth of 86 MHz) and/or a low-resolution (1440 channels with a total bandwidth of 1 GHz) acousto-optical spectrometer (AOS). The image-band suppression is typically $>$20 dB in the λ=3 and 2 mm bands, and $>$15 dB in the λ=1.3 mm band. Typical system temperatures (expressed in the T_A^* scale) for the 3mm and 2mm SIS receivers were 120–180 K in the 85–100 and 135–150 GHz bands. In the 100–115 GHz range the temperatures were 200–300 K. The system temperatures for the new 1.3mm receiver were around 200, 350, and 900 K at 210–220, 230, and 265 GHz, respectively. At 345 GHz, the system temperature was 800–1000 K. Dual beam-switching (beam-throw $\approx$12′ in azimuth) was used throughout. The intensity calibration was done with the chopper-wheel method. Pointing and focus checks were made towards the Orion KL SiO maser, and the stellar SiO masers R Dor, U Men, AH Sco, VX Sgr, and W Hya. The pointing errors were typically 3″ rms in each coordinate. Calibration uncertainties are estimated to be $\pm10\%, \pm15\%$, $\pm20\%$ and $\pm25\%$ in the λ=3, 2, 1.3, and 0.8 mm bands, respectively. The total uncertainties in the observed intensities are then obtained by adding quadratically the contribution of noise in the spectra to the pointing and calibration uncertainties. The CO(J=1–0) and CS(J=3–2) lines in N159W and N27 were observed during several observing runs as intensity checks in the λ=3 and 2 mm bands. Also, although not at every observing run, the Orion KL SiO maser was used as a calibration source.

[1] The Swedish–ESO Submillimetre Telescope (SEST) is operated jointly by ESO and the Swedish National Facility for Radio Astronomy, Onsala Space Observatory at Chalmers University of Technology.

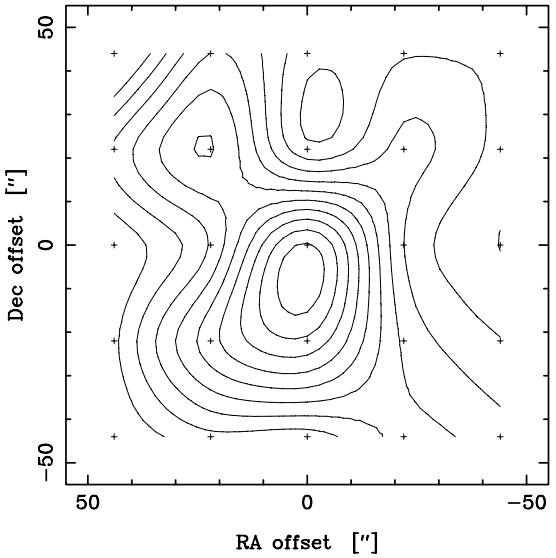

Fig. 1. Contour map of the CO(J=3–2) line emission, integrated between 105 and 125 km s^{-1}, in the N27 cloud. The offsets are relative to $\alpha(1950.0)$=00$^{\rm h}$46$^{\rm m}$32.9$^{\rm s}$, $\delta(1950.0)$=−73°21′50″. The contour levels, given on the main-beam brightness scale, are from 1.7 to 17 K km s^{-1} in steps of 1.7 K km s^{-1}. The grid spacing is 22″, and the noise-level in the individual spectra is typically 1.4 K km s^{-1} (2σ).

4. Results

4.1. Observational data

Spectra of the observed lines are shown[2] in Figs. 2–14. A contour map of the integrated intensity of the CO(J=3–2) line emission in N27 is displayed in Fig. 1. We have also mapped the CO(J=1–0 and 2–1), and ^{13}CO(J=2–1) line emission in N27; CO(J=2–1), and ^{13}CO(J=2–1) in N159S; ^{13}CO(J=2–1) in N160; the maps are shown in Heikkilä (1998). In addition, we have made small maps of the HCO$^+$(J=1–0) line emission in N27, N160 and 30Dor-10; C$_2$H[$N(J,F)$=1($\frac{3}{2}$,2)-0($\frac{1}{2}$,1)] in N159W; and single-position observations of the HCO$^+$(J=1–0) line in N12 (also denoted LIRS 36), N66, N88 and SMC-B1, and the CS(J=3–2) line in N66, in the SMC [for coordinates see Rubio et al. (1996)]. Rubio et al. (1993, 1996) have published CO(J=1–0 and 2–1) and ^{13}CO(J=1–0) maps of N27. For the LMC objects, CO(J=1–0), and for 30Dor-10 and N159W also CO(J=3–2), maps can be found in Paper I and Johansson et al. (1998). Paper I contains line luminosities for a number of molecular species in N159W. The rest frequencies of the observed spectral lines, taken from Lovas (1992), are listed in Table 2. Tables 3–9 give the line parameters from fits of Gaussian line profiles to the measured spectra. In some cases, due to complex line profiles or low signal-to-noise ratios, only the integrated intensity, $\int T_{\rm mb}{\rm d}v$, is given. The upper limit for the integrated intensity of a non-detected line was calculated as $T_{\rm pp}\Delta v$, where $T_{\rm pp}$ is the peak-to-peak channel-noise in a spectrum which has been smoothed to a resolution equal to the expected full-width at half-maximum (FWHM) line-width, Δv. The intensities are expressed in the main-beam brightness temperature scale: $T_{\rm mb}$=$T_{\rm A}^*/\eta_{\rm mb}$, where $\eta_{\rm mb}$ is the measured main-beam efficiency of the telescope: 0.75, 0.70, 0.66, and 0.60 at 86, 115, 147, and 230 GHz, respectively. At 345 GHz we used $\eta_{\rm mb}$=0.33, see Johansson et al. (1998). Usually the low-resolution spectrometer was used for the λ=2 and 1.3 mm observations and the high-resolution spectrometer for the λ=3 mm observations. The channel-separations are 1.4 and 0.90 km s^{-1} (at 145 and 230 GHz, respectively) for the low-resolution AOS, and 0.13 km s^{-1} (at 100 GHz) for the high-resolution AOS. During the data reduction the spectra obtained with the high-resolution AOS were smoothed to resolutions of ≈0.5 km s^{-1}. The velocity scale in the spectra is relative to the local standard of rest (LSR). The tabulated channel-noises ($T_{\rm rms}$) and uncertainties in the integrated intensities ($I_{\rm rms}$) are defined by 2σ rms noise fluctuations. The rms noise in the integrated intensity of a detected line was calculated using the expression $I_{\rm rms}$=$\sqrt{n_{\rm chan}}\,\Delta v_{\rm chan}\,T_{\rm rms}$, where $n_{\rm chan}$ is twice the FWHM line-width in number of channels, $\Delta v_{\rm chan}$ is the channel-separation in km s^{-1}, and $T_{\rm rms}$ is the channel-noise at 2σ level.

Ratios of velocity-integrated line-intensities are given in Tables 10–11. When computing intensity ratios, the intensities were corrected for large-scale beam-dilution by taking into account the angular size of the source relative to the size of the telescope-beam. Where possible, generally only in N159W, we used the convolution-method described in Paper I. In cases with limited map information we assumed that the radial intensity distribution of the cloud is Gaussian. The intensities in the centre-position of the cloud can then be expressed as I_0=$I_{\rm mb}/\eta_{\rm bf}$, where $\eta_{\rm bf}$=$\Theta^2_{\rm source}/(\Theta^2_{\rm mb}+\Theta^2_{\rm source})$ is the 'Gaussian' beam-filling factor, and $\Theta_{\rm source}$ and $\Theta_{\rm mb}$ are the FWHM sizes of the source and the main-beam of the telescope, respectively. A comparison of intensity ratios obtained with these two methods in N159W shows a good agreement. The source sizes were determined from maps of different molecules and transitions. For the N159W cloud, all mapped molecules – except ^{12}CO and possibly HCO$^+$ – indicate a de-convolved source size of ≈40″. The ^{12}CO size is ≈65″, whereas the HCO$^+$ sizes are ≈60″ and ≈40″ as traced by the J=1–0 and J=3–2 lines, respectively. In the analysis we applied the smaller source size to all molecules (including HCO$^+$) except ^{12}CO. In the other clouds we generally lack good quality maps for other molecules than ^{12}CO and ^{13}CO. Similarly to N159W, these clouds have a ^{13}CO line emission which is less extended than that of ^{12}CO. In the analysis, we assumed that the source size of 'non-^{12}CO' species is identical to that of ^{13}CO. In 30Dor-27 we lack information on the ^{13}CO size, and used a source size of $\frac{2}{3}\times$CO-size for other species than ^{12}CO. In N27, the CO(J=1–0 and 2–1) maps indicate a de-convolved source size of 70″, while the J=3–2 map suggests 60″. The applied source sizes are given in Table 13. We generally apply $\pm30\%$ uncertainties to all intensity ratios used in the estimation of gas temperatures, gas densities, and molecular abundances; exceptions are the H$_2$CO($3_{0,3}$–$2_{0,2}$/$3_{2,2}$–$2_{2,1}$) ratio in N159W and the HCO$^+$(J=1–0)/H^{13}CO$^+$(J=1–0) ratio in N27 and 30Dor-10 (see Sects. 4.3.2 and 5.2.8).

[2] Figs. 3–14 are only available in the electronic version of this paper.

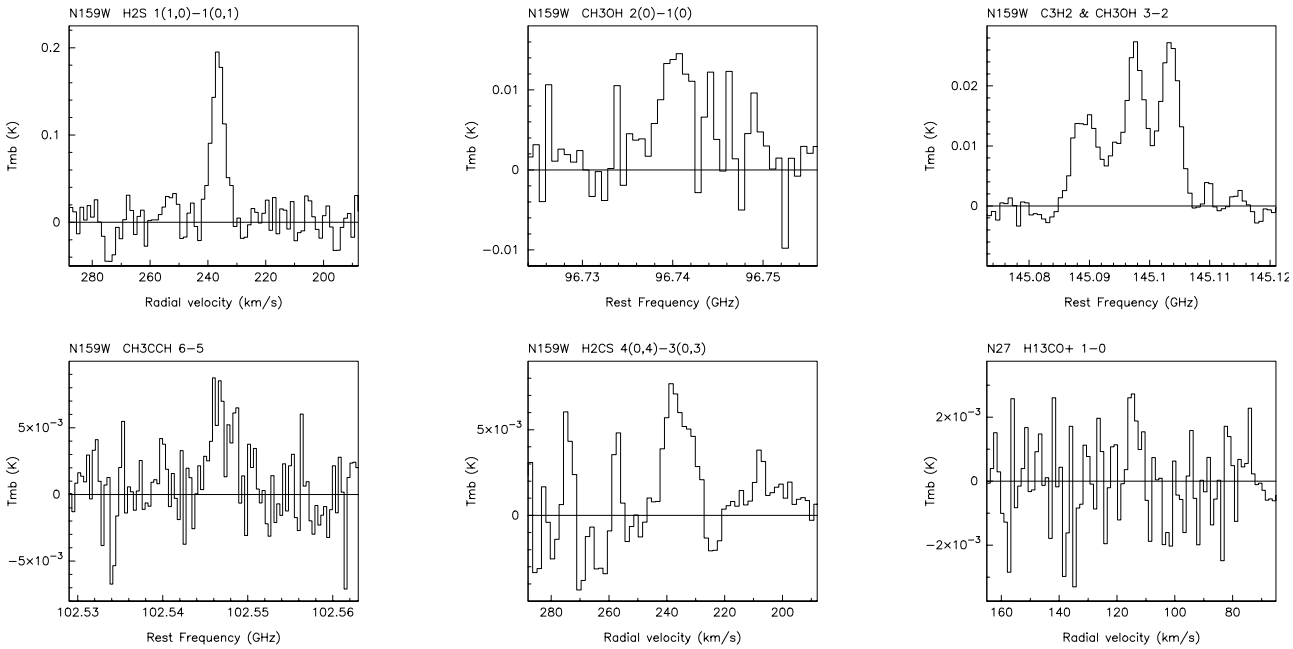

Fig. 2. Spectra of new detections in the LMC and the SMC. The intensities are expressed as main-beam brightness temperatures and the velocities are relative to the local standard of rest.

4.2. New detections

The number of definitely detected interstellar molecules now (December 1998) amounts to 16 (26 including isotopomers) in the LMC and 10 (14 including isotopomers) in the SMC, respectively (Huggins et al. 1975; Whiteoak & Gardner 1976a, 1976b; Whiteoak et al. 1980; Batchelor et al. 1981; Caswell & Haynes 1981; Scalise & Braz 1982; Koornneef & Israel 1985; Israel & Koornneef 1988; Johansson 1991; Sinclair et al. 1992; Paper I; Chin et al. 1996b, 1997, 1998; this paper). Furthermore, there are two tentative detections, viz. $C^{34}S$ (Chin et al. 1998) in the SMC, and para-H_2CS (this paper) in the LMC. Here we report on the detections of spectral line emission from $H^{13}CO^+$ in N27 in the SMC, and from hydrogen sulphide (ortho-H_2S; the first detection in an external galaxy), methanol (CH_3OH; thermal emission) and methyl acetylene (CH_3CCH) in N159W in the LMC (see Fig. 2). The detected ortho-H_2S($J_{K_\mathrm{p},K_\mathrm{o}}$=$1_{1,0}$–$1_{0,1}$) line at $\nu\approx$168.8 GHz is the ortho ground-state transition. The detected methanol lines are J=2–1 and 3–2 lines at $\nu\approx$96.7 and ≈145.1 GHz, respectively. In particular, the two 145.1 GHz lines are very convincing. We did not detect a few additional methanol lines with rest-frequencies near 145.1 GHz. The energies of the upper levels of the undetected lines are 34–50 K, which can explain the non-detections, since the upper state energy of detected lines in the LMC sources is typically $<$30 K. An alternative explanation could be anomalous excitation.

4.3. Physical state of the molecular gas

4.3.1. General remarks

A summary of the estimates of the physical state of the molecular gas, viz. the kinetic temperature [T_kin] and the number density of molecular hydrogen [$n(\mathrm{H_2})$], along with other global cloud parameters (average gas density, cloud size, virial mass, column density of H_2, and visual extinction) is given in Table 13. The estimates of T_kin and $n(\mathrm{H_2})$ using individual tracers are presented in Tables 14–15. The estimation of T_kin and $n(\mathrm{H_2})$ was made by applying a statistical-equilibrium excitation and radiative transfer code to ratios of observed velocity-integrated line intensities (Tables 10–11). The radiative transfer was treated in the mean escape probability (MEP) approximation and the model cloud was spherical with a constant density and temperature. The used model was developed by J.H. Black and is described in e.g. Jansen et al. (1994). The ambient radiation field was taken to be the cosmic background radiation, i.e., a black body at a temperature of 2.73 K. For most of the species, the applied electric dipole moments and references for collision coefficients can be found in Jansen et al. (1994). For CN we used collision coefficients calculated by P. Bergman (see Olofsson et al. 1996), while for C_2H we used those of HCN. The excitation of trace molecules by collisions with electrons was not taken into account. This because the fractional abundance of electrons in N159W has been estimated to be less than 10^{-5} (Heikkilä et al. 1997a). Furthermore, using C^+ data from Israel et al. (1996), we estimate[3], the C^+ abundance (which is often assumed to be similar to the electron abundance) to be typically a few$\times10^{-5}$ in N159W, N160 and 30Dor-10 areas. However, the distributions of C^+ and CO are not fully coextensive, e.g. their peak positions differ.

In addition to the observational data presented in this paper, we have taken data from Paper I and Johansson et al. (1998). In the temperature estimation we also employed the local thermo-

[3] We applied Eq. (6) with S_mol=S_{C^+}=S_CO.

Table 2. Rest frequencies of observed spectral lines

Molecule	Transition	Rest frequency [MHz]	Molecule	Transition	Rest frequency [MHz]
CO	J=1–0	115271.204	SO_2	$J_{K_p,K_o}=8_{1,7}–8_{0,8}$	83688.086
CO	J=2–1	230538.000	SO_2	$J_{K_p,K_o}=3_{1,3}–2_{0,2}$	104029.416
CO	J=3–2	345795.991			
^{13}CO	J=1–0	110201.353	OCS	J=11–10	133785.897
^{13}CO	J=2–1	220398.686			
C^{18}O	J=2–1	219560.319	o-H_2S	$J_{K_p,K_o}=1_{1,0}–1_{0,1}$	168762.762
C^{17}O	J=2–1	224714.368			
			HDO	$J_{K_p,K_o}=1_{1,0}–1_{1,1}$	80578.283
HCO^+	J=1–0	89188.518			
HCO^+	J=3–2	267557.625	C_2H	$N(J,F)$=1($\frac{3}{2}$,2)–0($\frac{1}{2}$,1)	87316.925
H^{13}CO$^+$	J=1–0	86754.294	C_2H	$N(J,F)$=1($\frac{3}{2}$,1)–0($\frac{1}{2}$,0)	87328.624
DCO^+	J=2–1	144077.321	C_2H	$N(J,F)$=1($\frac{1}{2}$,1)–0($\frac{1}{2}$,1)	87402.004
			C_2H	$N(J,F)$=1($\frac{1}{2}$,0)–0($\frac{1}{2}$,1)	87407.165
CN	$N(J,F)$=1($\frac{1}{2}$,$\frac{1}{2}$)–0($\frac{1}{2}$,$\frac{3}{2}$)	113144.192			
CN	$N(J,F)$=1($\frac{1}{2}$,$\frac{3}{2}$)–0($\frac{1}{2}$,$\frac{1}{2}$)	113170.528	o-H_2CO	$J_{K_p,K_o}=2_{1,2}–1_{1,1}$	140839.518
CN	$N(J,F)$=1($\frac{1}{2}$,$\frac{3}{2}$)–0($\frac{1}{2}$,$\frac{3}{2}$)	113191.317	o-H_2CO	$J_{K_p,K_o}=2_{1,1}–1_{1,0}$	150498.339
CN	$N(J,F)$=1($\frac{3}{2}$,$\frac{3}{2}$)–0($\frac{1}{2}$,$\frac{1}{2}$)	113488.140	p-H_2CO	$J_{K_p,K_o}=2_{0,2}–1_{0,1}$	145602.953
CN	$N(J,F)$=1($\frac{3}{2}$,$\frac{5}{2}$)–0($\frac{1}{2}$,$\frac{3}{2}$)	113490.982	o-H_2CO	$J_{K_p,K_o}=3_{1,3}–2_{1,2}$	211211.452
CN	$N(J,F)$=1($\frac{3}{2}$,$\frac{1}{2}$)–0($\frac{1}{2}$,$\frac{1}{2}$)	113499.639	p-H_2CO	$J_{K_p,K_o}=3_{0,3}–2_{0,2}$	218222.191
CN	$N(J,F)$=1($\frac{3}{2}$,$\frac{3}{2}$)–0($\frac{1}{2}$,$\frac{3}{2}$)	113508.944	p-H_2CO	$J_{K_p,K_o}=3_{2,2}–2_{2,1}$	218475.639
CN	$N(J,F)$=2($\frac{3}{2}$,$\frac{5}{2}$)–1($\frac{3}{2}$,$\frac{5}{2}$)	226359.987	p-H_2CO	$J_{K_p,K_o}=3_{2,1}–2_{2,0}$	218760.068
CN	$N(J,F)$=2($\frac{3}{2}$,$\frac{5}{2}$)–1($\frac{1}{2}$,$\frac{3}{2}$)	226659.543	o-H_2CO	$J_{K_p,K_o}=3_{1,2}–2_{1,1}$	225697.772
CN	$N(J,F)$=2($\frac{3}{2}$,$\frac{1}{2}$)–1($\frac{1}{2}$,$\frac{1}{2}$)	226663.685			
CN	$N(J,F)$=2($\frac{5}{2}$,$\frac{5}{2}$)–1($\frac{3}{2}$,$\frac{3}{2}$)	226874.764	p-H_2CS	$J_{K_p,K_o}=4_{0,4}–3_{0,3}$	137371.043
HCN	$J(F)$=1(1)–0(1)	88630.416	o–c–C_3H_2	$J_{K_p,K_o}=2_{1,2}–1_{0,1}$	85338.905
HCN	$J(F)$=1(2)–0(1)	88631.847	o–c–C_3H_2	$J_{K_p,K_o}=3_{1,2}–2_{2,1}$	145089.595
HCN	$J(F)$=1(0)–0(1)	88633.936	p–c–C_3H_2	$J_{K_p,K_o}=4_{0,4}–3_{1,3}$	150820.669
HCN	J=3–2	265886.432	o–c–C_3H_2	$J_{K_p,K_o}=4_{1,4}–3_{0,3}$	150851.901
HNC	J=1–0	90663.543	HC_3N	J=16–15	145560.946
CS	J=2–1	97980.968	CH_3OH	$J_k=2_{-1}–1_{-1}$ E	96739.39
CS	J=3–2	146969.049	CH_3OH	$J_k=2_0–1_0$ A^+	96741.42
CS	J=5–4	244935.606	CH_3OH	$J_k=2_0–1_0$ E	96744.58
^{13}CS	J=3–2	138739.309	CH_3OH	$J_k=2_1–1_1$ E	96755.51
C^{34}S	J=3–2	144617.147	CH_3OH	$J_k=3_{-1}–2_{-1}$ E	145097.47
			CH_3OH	$J_k=3_0–2_0$ A^+	145103.23
SO	$J_N=3_2–2_1$	99299.879			
SO	$J_N=4_3–3_2$	138178.648	CH_3CCH	$J_K=6_2–5_2$	102540.144
SO	$J_N=6_5–5_4$	219949.391	CH_3CCH	$J_K=6_1–5_1$	102546.024
^{34}SO	$J_N=3_2–2_1$	97715.388	CH_3CCH	$J_K=6_0–5_0$	102547.984
^{34}SO	$J_N=4_3–3_2$	135775.633	CH_3CCH	$J_K=8_2–7_2$	136717.560
			CH_3CCH	$J_K=8_1–7_1$	136725.397
			CH_3CCH	$J_K=8_0–7_0$	136728.010

Table 3. Line parameters of the observed spectral lines in N159W

Molecule	Transition	$T_{\rm mb}$ [K]	$v_{\rm LSR}$ [km s^{-1}]	Δv [km s^{-1}]	$I^{\rm a}_{\rm mb}$ [K km s^{-1}]	$T^{\rm b}_{\rm rms}$ [K]
CN	$N(J,F)$=1($\frac{1}{2}$,$\frac{1}{2}$)–0($\frac{1}{2}$,$\frac{3}{2}$)	–	–	–	0.14	0.047
CN	$N(J,F)$=1($\frac{1}{2}$,$\frac{3}{2}$)–0($\frac{1}{2}$,$\frac{1}{2}$)	–	–	–	0.13	0.047
CN	$N(J,F)$=1($\frac{1}{2}$,$\frac{3}{2}$)–0($\frac{1}{2}$,$\frac{3}{2}$)	0.057	237.1	3.3	0.20(0.11)	0.047
CN	$N(J,F)$=1($\frac{3}{2}$,$\frac{3}{2}$)–0($\frac{1}{2}$,$\frac{1}{2}$)	0.056	236.3	4.9	0.29(0.067)	0.032
CN	$N(J,F)$=1($\frac{3}{2}$,$\frac{5}{2}$)–0($\frac{1}{2}$,$\frac{3}{2}$)	0.13	237.5	6.9	0.92(0.080)	0.016
CN	$N(J,F)$=1($\frac{3}{2}$,$\frac{1}{2}$)–0($\frac{1}{2}$,$\frac{1}{2}$)	0.032	237.3	9.3	0.32(0.092)	0.032
CN	$N(J,F)$=1($\frac{3}{2}$,$\frac{3}{2}$)–0($\frac{1}{2}$,$\frac{3}{2}$)	–	237.2	–	0.38(0.077)	0.032
CN	$N(J,F)$=1($\frac{3}{2}$,$\frac{3}{2}$)–0($\frac{1}{2}$,$\frac{1}{2}$); 1($\frac{3}{2}$,$\frac{5}{2}$)–0($\frac{1}{2}$,$\frac{3}{2}$)	–	–	–	1.23	0.016
CN	$N(J)$=1($\frac{1}{2}$)–0($\frac{1}{2}$)	–	–	–	0.47[c]	–
CN	$N(J)$=1($\frac{3}{2}$)–0($\frac{1}{2}$)	–	–	–	1.91[c]	–
CN	$N(J,F)$=2($\frac{3}{2}$,$\frac{5}{2}$)–1($\frac{3}{2}$,$\frac{5}{2}$)	0.022	236.9	10.3	0.24(0.084)	0.019
CN	$N(J,F)$=2($\frac{3}{2}$,$\frac{5}{2}$)–1($\frac{1}{2}$,$\frac{3}{2}$); 2($\frac{3}{2}$,$\frac{1}{2}$)–1($\frac{1}{2}$,$\frac{1}{2}$)	0.045	235.0	9.1	0.44(0.080)	0.019
CN	$N(J)$=2($\frac{3}{2}$)–1($\frac{1}{2}$)	–	–	–	0.63[c]	–
CN	$N(J)$=2($\frac{5}{2}$)–1($\frac{3}{2}$)	0.096	238.0	6.7	0.69(0.067)[c]	0.019
CN	N=1–0	–	–	–	2.92[d]	–
CN	N=2–1	–	–	–	1.55[d]	–
CS	J=3–2	0.27	237.7	8.2	2.38(0.13)	0.027
^{13}CS	J=3–2	0.012	237.7	7.2	0.092(0.027)	0.0058
C^{34}S	J=3–2	0.021	237.4	6.3	0.15(0.029)	0.0064
SO	J_N=4_3–3_2	0.13	235.5	7.3	1.00(0.029)	0.058
SO	J_N=6_5–5_4	0.081	236.8	5.9	0.51(0.051)	0.015
o-H$_2$S	$J_{K_{\rm p},K_{\rm o}}$=$1_{1,0}$–$1_{0,1}$	0.19	236.5	5.3	1.07(0.22)	0.057
C$_2$H	$N(J,F)$=1($\frac{1}{2}$,1)–0($\frac{1}{2}$,1)	0.071	236.6	7.5	0.57(0.083)	0.028
C$_2$H	$N(J,F)$=1($\frac{1}{2}$,0)–0($\frac{1}{2}$,1)	0.039	237.3	5.7	0.24(0.073)	0.028
C$_2$H	$N(J,F)$=1($\frac{3}{2}$,2)–0($\frac{1}{2}$,1)	0.14	237.6	7.9	1.18(0.11)	0.034
C$_2$H	$N(J,F)$=1($\frac{3}{2}$,1)–0($\frac{1}{2}$,0)	0.087	237.4	7.4	0.68(0.099)	0.034
C$_2$H	N=1–0	–	–	–	2.92[d]	–
o-H$_2$CO	$J_{K_{\rm p},K_{\rm o}}$=$2_{1,2}$–$1_{1,1}$	0.21	237.5	8.0	1.81(0.092)	0.019
o-H$_2$CO	$J_{K_{\rm p},K_{\rm o}}$=$2_{1,1}$–$1_{1,0}$	0.16	237.7	7.6	1.27(0.098)	0.021
p-H$_2$CO	$J_{K_{\rm p},K_{\rm o}}$=$2_{0,2}$–$1_{0,1}$	0.13	237.7	7.7	1.04(0.030)	0.0062
o-H$_2$CO	$J_{K_{\rm p},K_{\rm o}}$=$3_{1,3}$–$2_{1,2}$	0.10	237.5	6.7	0.74(0.088)	0.024
p-H$_2$CO	$J_{K_{\rm p},K_{\rm o}}$=$3_{0,3}$–$2_{0,2}$	0.088	236.1	7.6	0.71(0.027)	0.0068
p-H$_2$CO	$J_{K_{\rm p},K_{\rm o}}$=$3_{2,2}$–$2_{2,1}$	0.012	236.6	5.9	0.077(0.024)	0.0068
p-H$_2$CO	$J_{K_{\rm p},K_{\rm o}}$=$3_{2,1}$–$2_{2,0}$	0.013	237.4	5.2	0.074(0.023)	0.0068
o-H$_2$CO	$J_{K_{\rm p},K_{\rm o}}$=$3_{1,2}$–$2_{1,1}$	0.10	237.5	7.2	0.78(0.070)	0.019
o–c–C$_3$H$_2$	$J_{K_{\rm p},K_{\rm o}}$=$2_{1,2}$–$1_{0,1}$	0.061	237.2	7.6	0.49(0.068)	0.022
o–c–C$_3$H$_2$	$J_{K_{\rm p},K_{\rm o}}$=$3_{1,2}$–$2_{2,1}$	0.015	235.6	9.2	0.14(0.043)	0.0042
p–c–C$_3$H$_2$	$J_{K_{\rm p},K_{\rm o}}$=$4_{0,4}$–$3_{1,3}$	0.017	236.9	8.6	0.16(0.054)	0.011
o–c–C$_3$H$_2$	$J_{K_{\rm p},K_{\rm o}}$=$4_{1,4}$–$3_{0,3}$	0.019	237.7	8.9	0.18(0.054)	0.011
CH$_3$OH	J_k=2–1 E	0.015	239.6	10.7	0.18(0.057)	0.0098
CH$_3$OH	J_k=3_{-1}–2_{-1} E	0.026	235.6	7.6	0.21(0.040)	0.0042
CH$_3$OH	J_k=3_0–2_0 A$^+$	0.028	235.5	7.6	0.22(0.040)	0.0042

Table 3. (continued)

Molecule	Transition	$T_{\rm mb}$ [K]	$v_{\rm LSR}$ [km s^{-1}]	Δv [km s^{-1}]	$I^{\rm a}_{\rm mb}$ [K km s^{-1}]	$T^{\rm b}_{\rm rms}$ [K]
CH_3CCH	J=6–5 (K=0–1)	0.007	236.7	–	0.065(0.023)	0.0050
CH_3CCH	J=6–5 (K=0–2)	–	–	–	0.080	0.0050
CH_3CCH	J=8–7 (K=0–2)	0.005	237.1	–	0.080	0.0042

[a] The numbers in brackets are 2σ noise fluctuations.
[b] 2σ rms noise.
[c] Total intensity of the observed hyperfine structure (hfs) lines.
[d] Total intensity. Not observed hfs components have been accounted for by assuming LTE.

Table 4. Undetected and tentatively detected transitions in N159W

Molecule	Transition	$T_{\rm mb}$ [K]	$v_{\rm LSR}$ [km s^{-1}]	Δv [km s^{-1}]	$I_{\rm mb}$ [K km s^{-1}]	$T^{\rm a}_{\rm rms}$ [K]
^{34}SO	J_N=3_2–2_1	–	–	–	<0.14	0.019
^{34}SO	J_N=4_3–3_2	–	–	–	<0.080[c]	0.0062
SO_2	$J_{K_{\rm p},K_{\rm o}}$=$8_{1,7}$–$8_{0,8}$	–	–	–	<0.054	0.017
SO_2	$J_{K_{\rm p},K_{\rm o}}$=$3_{1,3}$–$2_{0,2}$	–	–	–	<0.080	0.0098
OCS	J=11–10	–	–	–	<0.14	0.0090
HDO	$J_{K_{\rm p},K_{\rm o}}$=$1_{1,0}$–$1_{1,1}$	–	–	–	<0.44	0.034
p-H_2CS	$J_{K_{\rm p},K_{\rm o}}$=$4_{0,4}$–$3_{0,3}$	0.0072	236.2	10.6	0.081(0.024)[b]	0.0042
HC_3N	J=16–15	–	–	–	<0.087	0.0062

[a] 2σ rms noise.
[b] Tentative detection.
[c] A very tentative detection. A formal Gaussian fit gives $I_{\rm mb}\approx$0.045 K km s^{-1}.

dynamic equilibrium (LTE) approach as a complement to the MEP analysis. The basic assumptions in the LTE approach are a uniformly excited and Boltzmann distributed population of the rotational energy levels and low optical depths for the emitted line radiation, see e.g. Turner (1991).

4.3.2. Gas temperature

Johansson et al. (1998) made estimates of the gas temperature in N159W, 30Dor-10, and 30Dor-27 using ^{12}CO and ^{13}CO multi-transition data and a MEP analysis. Here we present results for N159S, N160 and N27 using the same approach. For N159W we used other temperature probes as well. The nominal gas temperatures obtained from CO analysis are typically $\sim$20 K for most of the clouds.

The MEP solutions for N159W using the multi-transition data of ^{12}CO, ^{13}CO, C^{18}O, and C^{17}O give 20$\pm$5 K for densities $>10^3$ cm^{-3}. For densities of a few$\times10^2$–10^3 cm^{-3} the CO isotopomer data allow temperatures up to $\sim$100 K. The CO(J=1–0, 2–1, and 3–2) LTE excitation temperatures (corrected for $\eta_{\rm mb}$ and $\eta_{\rm bf}$, and assuming optically thick line emission), which should provide a lower limit to the kinetic temperature, yield $T_{\rm kin}>$14 K.

In principle, symmetric top molecules are good temperature probes. This class of molecules exhibits line emission emerging from states which are predominantly collisionally populated and have significantly different energies, with lines often close in frequency. In such cases, the lines can be observed simultaneously with the same receiver and the same spectrometer, implying reduced observational uncertainties (e.g. same pointing offsets, same calibration uncertainties, and similar spatial resolution). Our attempts to observe the J=6–5 and 8–7 lines of methyl acetylene (CH_3CCH) resulted in marginal detections. The lines are very weak. At best, the resulting signal-to-noise ratio allows an upper limit for the excitation temperature for the E-symmetry species of CH_3CCH to be estimated from the K=1 and 2 components of the J=6–5 line. The K=0 (A-symmetry) and K=1 (E-symmetry) components of the J=6–5 line are blended in the observed spectrum. Assigning equal intensities (0.0325 K km s^{-1}) to each of them and setting 0.015 K km s^{-1} for the K=2 component (cf. Table 3) gives $T_{\rm kin}<$31 K. Formaldehyde (H_2CO) lines, in particular those at $\nu\approx$218 GHz, are also useful in temperature estimation. The energy levels of H_2CO, a slightly asymmetric top, are described by three quantum numbers: the total angular momentum (J), and the projections of J along the symmetry axis of the molecule in the limits of a prolate and an oblate symmetric top ($K_{\rm p}$ and $K_{\rm o}$, respectively). The energy level structure of formaldehyde can be organised in ladders with fixed K values, each ladder behaving like a linear rotor. Since rapid radiative transitions between two K-ladders

Table 5. Line parameters of the observed spectral lines in N159S

Molecule	Transition	$T_{\rm mb}$ [K]	$v_{\rm LSR}$ [km s^{-1}]	Δv [km s^{-1}]	$I^{\rm a}_{\rm mb}$ [K km s^{-1}]	$T^{\rm b}_{\rm rms}$ [K]
CO	J=1–0[d]	6.1	235.4	7.5	49.0	–
CO	J=2–1	4.75	235.1	8.1	40.8(0.81)	0.43
CO	J=3–2	4.82	235.3	7.0	35.8(1.3)	0.44
^{13}CO	J=1–0[d]	0.72	235.5	5.9	4.5	–
^{13}CO	J=2–1	0.89	235.9	6.3	5.96(0.56)	0.11
CN	$N(J,F)$=1($\frac{3}{2},\frac{5}{2}$)–0($\frac{1}{2},\frac{3}{2}$)	–	–	–	$<$0.15	0.051
CN	N=1–0	–	–	–	$<$0.45[c]	–
CS	J=2–1	0.15	235.4	6.6	1.04(0.084)	0.032
CS	J=3–2	0.034	235.0	7.9	0.28(0.11)	0.021
SO	J_N=3_2–2_1	0.038	234.4	6.2	0.25(0.061)	0.017
SO	J_N=4_3–3_2	0.022	235.2	6.0	0.14(0.054)	0.013
HCO^+	J=1–0	0.10	235.0	7.7	0.84(0.065)	0.022
HCN	J=1–0[d]	0.06	–	7.2	0.46	–
HNC	J=1–0	0.027	235.6	4.6	0.13(0.053)	0.016
C_2H	$N(J,F)$=1($\frac{3}{2}$,2)–0($\frac{1}{2}$,1)	0.048	235.2	6.8	0.35(0.037)	0.014
C_2H	$N(J,F)$=1($\frac{3}{2}$,1)–0($\frac{1}{2}$,0)	0.027	234.9	7.6	0.22(0.039)	0.014
C_2H	N=1–0	–	–	–	0.91[c]	–
o-H_2CO	$J_{K_{\rm p},K_{\rm o}}$=$2_{1,2}$–$1_{1,1}$	0.031	237.0	8.5	0.28(0.074)	0.014
o-H_2CO	$J_{K_{\rm p},K_{\rm o}}$=$2_{1,1}$–$1_{1,0}$	0.026	236.0	8.6	0.23(0.057)	0.012
p-H_2CO	$J_{K_{\rm p},K_{\rm o}}$=$2_{0,2}$–$1_{0,1}$	0.022	234.6	8.7	0.20(0.064)	0.013

[a] The numbers in brackets are 2σ noise fluctuations.
[b] 2σ rms noise.
[c] Total intensity. Not observed hfs components have been accounted for by assuming LTE.
[d] Data taken from Johansson et al. (1994; 1998).

are forbidden, the excitation between K-ladders is mainly governed by collisions and, provided that optical depth effects can be accounted for, reflects the kinetic temperature of the gas. In N159W, the observed ($3_{0,3}$–$2_{0,2}$)/($3_{2,2}$–$2_{2,1}$) intensity ratio of 9.2±2.0 (we have added the 2σ noise fluctuations for the two lines in question, which were observed simultaneously with the same receiver and the same spectrometer, quadratically) indicates $T_{\rm kin}$=29±5 K using the following LTE expression (e.g. Mangum & Wootten 1993):

$$T_{\rm kin}[{\rm K}] = \frac{47.1}{\ln\left(0.556\frac{I_0(3_{0,3}-2_{0,2})}{I_0(3_{2,2}-2_{2,1})}\right)} \quad (1)$$

while the MEP analysis gives $T_{\rm kin}$=30±3 K. Heikkilä et al. (1997a) estimated the temperature using deuterium fractionation and obtained 25±2 K (a simplistic fractionation consideration) and 10–24 K [comparison with a model for a Galactic dark cloud from Millar et al. (1989)]. Strictly speaking, deuterium fractionation only gives an upper limit to the temperature. A weighted average of 30±3, 25±2 and 20±5 K gives $T_{\rm kin}$=26±2 K in N159W. However, we adopt a more conservative view and estimate the gas temperature in N159W to be 25±10 K.

Also, the ortho-to-para (o/p) ratio in formaldehyde and cyclo-propenylidene (c-C_3H_2), and the ratio between the A- and E-symmetry species (A/E) of methanol can be used as temperature probes. More precisely, these ratios carry information of the temperature that prevailed when these molecules were formed. The two latter ratios were only measured in N159W. The o/p ratio in H_2CO varies slightly among the sources, the average being 2.6. This is close to the high-temperature limit of 3. Assuming thermodynamic equilibrium, the ratio in N159W (1.8) indicates that H_2CO was formed in an environment with a temperature $>$12 K. In N27, we infer an H_2CO o/p ratio of ≈2.4, implying a formation temperature of $>$16 K. Further, we estimate an o/p ratio of 3.3 in the N12 cloud (also denoted LIRS 36) in the SMC using data from Chin et al. (1998). [The applied cloud parameters for N12 are given in Sect. 5.2.4]. Hence, concerning the o/p ratio in H_2CO, no obvious difference between the LMC and the SMC is apparent. In N159W, the o/p ratio in c-C_3H_2 is ≈0.7. Turner et al. (1998) finds an average ratio of 2.3 in a sample of small translucent clouds in the Galaxy. The energy difference between the ground-states of the ortho and the para species is only 2.35 K (Turner 1991), and accordingly the high temperature limit of 3 in the o/p ratio should be reached already at low temperatures. Therefore, unless c-C_3H_2 was formed at a very low temperature in N159W, the o/p ratio in c-C_3H_2 appears to be lower than expected. However, a low o/p ratio may be explained by non-LTE excitation. The only observed para line in N159W is the $J_{K_{\rm p},K_{\rm o}}$=$4_{0,4}$–$3_{1,3}$ transition at ν≈150.82 GHz. The intensity ratio between the $J_{K_{\rm p},K_{\rm o}}$=$4_{1,4}$–$3_{0,3}$ (ortho) line

Table 6. Line parameters of the observed spectral lines in N160

Molecule	Transition	$T_{\rm mb}$ [K]	$v_{\rm LSR}$ [km s^{-1}]	Δv [km s^{-1}]	$I^{\rm a}_{\rm mb}$ [K km s^{-1}]	$T^{\rm b}_{\rm rms}$ [K]
CO	J=1–0	2.93	237.6	5.1	15.8(1.0)	0.43
^{13}CO	J=1–0	0.34	237.8	4.6	1.64(0.16)	0.072
^{13}CO	J=2–1	1.1	237.9	5.6	6.47(0.20)	0.063
CN	$N(J,F)$=1($\frac{3}{2},\frac{3}{2}$)–0($\frac{1}{2},\frac{1}{2}$)	0.083	236.2	1.2	0.11(0.043)	0.040
CN	$N(J,F)$=1($\frac{3}{2},\frac{5}{2}$)–0($\frac{1}{2},\frac{3}{2}$)	0.089	237.4	3.2	0.30(0.068)	0.040
CN	$N(J,F)$=1($\frac{3}{2},\frac{1}{2}$)–0($\frac{1}{2},\frac{1}{2}$)	–	–	–	$<$0.099	0.040
CN	$N(J,F)$=1($\frac{3}{2},\frac{3}{2}$)–0($\frac{1}{2},\frac{3}{2}$)	0.055	238.0	3.3	0.19(0.070)	0.040
CN	$N(J)$=1($\frac{3}{2}$)–0($\frac{1}{2}$)	–	–	–	0.64[c]	0.040
CN	N=1–0	–	–	–	1.08[d]	–
CS	J=2–1	0.11	237.7	4.7	0.56(0.12)	0.051
CS	J=3–2	0.11	237.4	6.6	0.75(0.11)	0.026
CS	J=5–4	0.051	238.0	5.1	0.28(0.071)	0.024
SO	J_N=4_3–3_2	0.095	237.4	4.9	0.50(0.074)	0.038
SO	J_N=6_5–5_4	0.062	237.9	3.6	0.23(0.11)	0.042
^{34}SO	J_N=4_3–3_2	–	–	–	$<$0.51	0.029
HCO^+	J=1–0	0.37	237.5	5.0	1.96(0.11)	0.044
HCO^+	J=3–2	0.19	236.5	7.2	1.45(0.40)	0.12
HCN	J=1–0	0.16	–	–	1.20(0.15)	0.032
C_2H	$N(J,F)$=1($\frac{3}{2}$,2)-0($\frac{1}{2}$,1)	0.13	238.0	2.8	0.39(0.17)	0.092
C_2H	N=1–0	–	–	–	0.94[d]	–
o-H_2CO	$J_{K_{\rm p},K_{\rm o}}$=$2_{1,2}$–$1_{1,1}$	0.17	237.3	4.9	0.88(0.078)	0.041
o-H_2CO	$J_{K_{\rm p},K_{\rm o}}$=$2_{1,1}$–$1_{1,0}$	0.12	237.3	6.7	0.86(0.098)	0.022
p-H_2CO	$J_{K_{\rm p},K_{\rm o}}$=$2_{0,2}$–$1_{0,1}$	0.15	237.6	5.0	0.81(0.091)	0.048

[a] The numbers in brackets are 2σ noise fluctuations.
[b] 2σ rms noise.
[c] Total intensity of the observed hyperfine structure (hfs) lines.
[d] Total intensity. Not observed hfs components have been accounted for by assuming LTE.

at ν≈150.85 GHz and the $J_{K_{\rm p},K_{\rm o}}$=$4_{0,4}$–$3_{1,3}$ line is 1.1. A low ($4_{1,4}$–$3_{0,3}$)/($4_{0,4}$–$3_{1,3}$) line intensity ratio (≈1.3) has also been observed in the Sgr B2 cloud (Vrtilek et al. 1987). Using the results of excitation and radiative transfer calculations of c-C_3H_2 by Avery & Green (1989), we find that the ($4_{1,4}$–$3_{0,3}$)/($4_{0,4}$–$3_{1,3}$) intensity ratio becomes significantly lower than 3 when the gas density is relatively high and the c-C_3H_2 abundance is low. For example, this ratio is between 1.8 and 1.1 if $T_{\rm kin}$=30 K, X(c-C_3H_2)/(dv/dR)=3×10^{-10} (km s^{-1} pc^{-1})$^{-1}$ and $n(H_2)$=10^5–10^6 cm^{-3}. A more accurate estimate of the c-C_3H_2 o/p ratio would be obtained by observing the stronger 3mm lines of the para species. The A/E ratio in methanol is expected to vary as $\exp(7.9/T_{\rm kin})$ due to the energy difference between the ground-states of the A and E species. The observed A/E ratio in N159W is 1.2–1.5 for $T_{\rm ex}$=5–10 K. This implies $T_{\rm kin}$=43–19 K, which is in agreement with the temperature estimates obtained from other probes. In Galactic sources, Menten et al. (1988) found A/E=1.3–2 in the Orion region, while Friberg et al. (1987) observed A/E=1.15–1.45 in dark clouds.

In N27 our estimate is 15±5 K, based on CO data only, while the HCO^+/DCO^+ ratio >19 indicates $T_{\rm kin}$>21 K.

In all sources, the *excitation* temperatures [$T_{\rm ex}$] for molecules with high electric dipole moments, such as CS, and within individual K-ladders of H_2CO usually are significantly lower than the kinetic temperature ($T_{\rm ex}$ being typically 5–10 K), indicating subthermal excitation. Similarly, higher transitions of CO isotopomers are subthermally excited, whereas the J=1 state is nearly thermalised. Exceptions are HCO^+ and C_2H. The MEP code indicates superthermal population ($T_{\rm ex}$>$T_{\rm kin}$) of the J=1 and N=1 levels, respectively, of these two molecules in some sources. This is the case e.g. in N159W. However, the resulting line intensity is not strongly affected since the optical depth

Table 7. Line parameters of the observed spectral lines in 30Dor-10

Molecule	Transition	$T_{\rm mb}$ [K]	$v_{\rm LSR}$ [km s^{-1}]	Δv [km s^{-1}]	$I_{\rm mb}^{\rm a}$ [K km s^{-1}]	$T_{\rm rms}^{\rm b}$ [K]
CO	J=1–0	1.60	249.7	15.0	25.4(2.7)	0.52
^{13}CO	J=1–0	0.095	250.4	9.7	0.99(0.19)	0.043
^{13}CO	J=2–1	0.28	–	–	2.89(0.20)	0.041
C^{18}O	J=2–1	$<$0.0056	–	–	$<$0.092(0.055)	0.0050
CN	$N(J,F)$=1($\frac{3}{2}$,$\frac{3}{2}$)–0($\frac{1}{2}$,$\frac{1}{2}$); 1($\frac{3}{2}$,$\frac{5}{2}$)–0($\frac{1}{2}$,$\frac{3}{2}$)	0.043	253.9	16.5	0.76(0.12)	0.020
CN	$N(J)$=1($\frac{3}{2}$)–0($\frac{1}{2}$)	–	–	–	1.2[c]	0.020
CN	N=1–0	–	–	–	1.66[d]	–
CS	J=2–1	0.056	250.5	13.0	0.78(0.16)	0.030
CS	J=3–2	0.072	252.4	10.0	0.77(0.12)	0.022
CS	J=5–4	0.040	–	–	0.38(0.11)	0.026
SO	J_N=4$_3$–3$_2$	0.012	250.1	17.9	0.23(0.057)	0.0078
SO	J_N=6$_5$–5$_4$	0.012	249.7	5.8	0.073(0.014)	0.0042
HCO$^+$	J=1–0	0.24	250.2	12.0	3.01(0.16)	0.027
HCO$^+$	J=3–2	0.10	–	–	1.50(0.26)	0.065
H^{13}CO$^+$	J=1–0	0.0064	250.0	10.4	0.071(0.040)	0.0058
HCN	J=1–0	0.068	251.7	15.4	1.12(0.16)	0.026
HNC	J=1–0	0.031	251.4	7.8	0.26(0.087)	0.020
C_2H	$N(J,F)$=1($\frac{3}{2}$,2)–0($\frac{1}{2}$,1)	0.036	250.4	14.5	0.56(0.14)	0.034
C_2H	$N(J,F)$=1($\frac{3}{2}$,1)–0($\frac{1}{2}$,0)	0.023	248.4	19.4	0.47(0.16)	0.034
C_2H	N=1–0	–	–	–	1.65[d]	–
o-H_2CO	$J_{K_{\rm p},K_{\rm o}}$=2$_{1,2}$–1$_{1,1}$	0.064	251.2	14.2	0.97(0.068)	0.010
o-H_2CO	$J_{K_{\rm p},K_{\rm o}}$=2$_{1,1}$–1$_{1,0}$	0.051	251.7	13.7	0.74(0.063)	0.010
p-H_2CO	$J_{K_{\rm p},K_{\rm o}}$=2$_{0,2}$–1$_{0,1}$	0.038	251.1	13.0	0.52(0.051)	0.0084
p-H_2CO	$J_{K_{\rm p},K_{\rm o}}$=3$_{0,3}$–2$_{0,2}$	0.025	–	–	0.26(0.063)	0.014
o-H_2CO	$J_{K_{\rm p},K_{\rm o}}$=3$_{1,2}$–2$_{1,1}$	$<$0.015	–	–	$<$0.21(0.077)	0.018
CH_3OH, c-C_3H_2	$\nu\approx$145.1 GHz	$<$0.019	–	–	$<$0.17(0.070)	0.010

[a] The numbers in brackets are 2σ noise fluctuations.
[b] 2σ rms noise.
[c] Total intensity of the observed hyperfine structure (hfs) lines.
[d] Total intensity. Not observed hfs components have been accounted for by assuming LTE.

decreases as $T_{\rm ex}$ increases. We compared the excitation temperatures for the various molecules and transitions obtained from the MEP analysis with those using the LTE approach. Generally the agreement is good.

4.3.3. Gas density

The gas density in the various clouds was constrained by multi-transition data of CS, SO, HCN, HCO$^+$ and H_2CO. In the estimation of the density, $\pm$30% uncertainties were applied to the intensity ratios given in Table 10 and the kinetic temperature was varied in a $\pm$5 K ($\pm$10 K in 30Dor-10) interval around the nominal temperature given in Table 13. Generally, solutions in the interval 10^4–10^6 cm^{-3} were found. This applies to all clouds. The nominal value for the density varies somewhat, but not dramatically, among the sources. For the temperature interval considered above, CO isotopomers typically give density estimates in the range 10^3–10^6 cm^{-3}. At higher temperatures also solutions for the density in the range 10^2–10^3 cm^{-3} can be found. Combining CS, SO and H_2CO data in N159W, we obtain (1–10)$\times10^5$ cm^{-3} for the dense gas-component in this source. In N27, a gas density of (5–50)$\times10^4$ cm^{-3} satisfies the estimates of all used 'high-density' probes.

Table 8. Line parameters of the observed spectral lines in 30Dor-27

Molecule	Transition	$T_{\rm mb}$ [K]	$v_{\rm LSR}$ [km s^{-1}]	Δv [km s^{-1}]	$I_{\rm mb}^{\rm a}$ [K km s^{-1}]	$T_{\rm rms}^{\rm b}$ [K]
CN	$N(J,F)$=1($\frac{3}{2},\frac{5}{2}$)–0($\frac{1}{2},\frac{3}{2}$)	<0.05	–	–	<0.10	0.040
CN	N=1–0	–	–	–	<0.30[c]	–
CS	J=2–1	–	–	–	0.47[d]	–
CS	J=3–2	–	–	–	0.33(0.070)	0.011
SO	J_N=3_2–2_1	<0.014	–	–	<0.20	0.0092
SO	J_N=4_3–3_2	0.020	240.4	5.1	0.11(0.034)	0.0086
HCO^+	J=1–0	–	–	–	0.57[d]	–
HCN	J=1–0	0.039	239.6	3.5	0.30(0.089)	0.022
C_2H	$N(J,F)$=1($\frac{3}{2}$,2)–0($\frac{1}{2}$,1)	0.050	–	–	0.38(0.11)	0.022
C_2H	$N(J,F)$=1($\frac{3}{2}$,1)–0($\frac{1}{2}$,0)	0.031	–	5.1	0.17(0.054)	0.022
C_2H	N=1–0	–	–	–	0.88[c]	–
o-H_2CO	$J_{K_{\rm p},K_{\rm o}}$=$2_{1,2}$–$1_{1,1}$	0.034	238.6	7.35	0.27(0.074)	0.032
o-H_2CO	$J_{K_{\rm p},K_{\rm o}}$=$2_{1,1}$–$1_{1,0}$	0.010	–	–	0.15(0.049)	0.012

[a] The numbers in brackets are 2σ noise fluctuations.
[b] 2σ rms noise.
[c] Total intensity. Not observed hfs components have been accounted for by assuming LTE.
[d] Data taken from Johansson et al. (1998).

4.4. Chemical composition of the molecular gas

4.4.1. Column densities

Molecular column densities were estimated with the same excitation/radiative transfer code as was used to estimate the physical state of the gas. The column density of a molecule 'mol' per unit line-width ($N_{\rm mol}/\Delta v$) was varied until the observed brightness temperature $T_{\rm R}$=$T_{\rm mb}/\eta_{\rm bf}$ (with $\eta_{\rm bf}$ as defined in Sect. 4.1) was obtained, while keeping $n({\rm H_2})$ and $T_{\rm kin}$ fixed at the values given in Table 13, see Table 16. We also present column density estimates using the LTE approach for all observed molecules in order to be able to judge the reliability of the results obtained for molecules for which *only* an LTE analysis was made (e.g., CH_3OH, H_2S), see Table 17. The MEP and the LTE results agree well in most cases. Expressions used in the LTE calculations are collected in Appendix A. For molecules with a resolved hyperfine structure (hfs), in our case CN and C_2H, we compensated for non-observed transitions by assuming relative intensities according to the optically thin LTE condition (Tucker et al. 1974; Skatrud et al. 1983) when calculating the total line intensity of the N=1–0 transition in the LTE case. Since the $N(J)$=1($\frac{1}{2}$)–0($\frac{1}{2}$) lines were observed only in one source (N159W), we have used the $N(J)$=1($\frac{3}{2}$)–0($\frac{1}{2}$) lines as a starting point in the calculation of the total CN(N=1–0) line intensity. For C_2H, the same procedure was done in the MEP analysis as well. The observed transitions show in most cases hfs line ratios close to their expected optically thin LTE values (relative deviations <20%, cf. the line ratios in N159W given in Table 12). In particular, this is true for C_2H, which may be explained by the rather large separation in frequency between the different hfs components, leading to only a small or no overlap of the lines. Accordingly, no radiative coupling, that could severely modify the populations and the intensities of the emerging radiation, will develop between the levels. Also for HCN the sum of the hfs lines in the J=1–0 transition was treated as a single line. The CN (1($\frac{3}{2}$)–0($\frac{1}{2}$))/ (1($\frac{1}{2}$)-0($\frac{1}{2}$)) fine structure line intensity ratio provides an interesting exception to the above quoted LTE conditions. The ratio in N159W is 4.1, which is significantly higher than the expected value of 2. In the Galaxy, line intensity ratios of 0.85–1.6 have been estimated for clouds near the Galactic Centre (Henkel et al. 1998) and 2.2 in Orion IRc2 (Olofsson et al. 1993), while a ratio of <2 is observed in circumstellar envelopes (Olofsson et al. 1993; Bachiller et al. 1997). In centres of starburst galaxies, Henkel et al. (1993, 1994, 1998) estimated a ratio of >1.6 in NGC 253, ≈1.5 in NGC 4945, ≈1.4 in IC 342 and ≈2.3 in M 82.

The tabulated column densities are 'peak' values in the sense that they have been corrected for large-scale beam-dilution, i.e., they apply for the column through the centre of the cloud. A possible small-scale beam-dilution (i.e. clumpiness) is not taken into account. 'Beam-averaged' values are recovered by multiplying the tabulated column densities with $\eta_{\rm bf}$.

4.4.2. Fractional abundances

In order to compare the chemical composition of the clouds and to investigate its possible dependence on the physical environment, we have estimated the fractional abundances of the

Table 9. Line parameters of the observed spectral lines in N27

Molecule	Transition	$T_{\rm mb}$ [K]	$v_{\rm LSR}$ [km s^{-1}]	Δv [km s^{-1}]	$I^{\rm a}_{\rm mb}$ [K km s^{-1}]	$T^{\rm b}_{\rm rms}$ [K]
CO	J=1–0	2.37	114.5	5.1	12.9(0.23)	0.21
CO	J=2–1	2.62	115.0	5.8	16.1(0.78)	0.24
CO	J=2–1 (1–0 beam)	1.71	114.6	6.6	12.1(0.28)	0.078
CO	J=3–2	2.70	114.7	5.4	15.5(1.44)	0.62
CO	J=3–2 (1–0 beam)	1.48	114.4	5.8	9.2(0.79)	0.33
^{13}CO	J=1–0	0.18	114.7	3.8	0.74(0.081)	0.085
^{13}CO	J=2–1	0.34	114.5	3.9	1.44(0.44)	0.11
C^{17}O	J=2–1	–	–	–	$<$0.032	0.0084
CN	$N(J,F)$=1($\frac{3}{2}$,$\frac{5}{2}$)–0($\frac{1}{2}$,$\frac{3}{2}$)	–	–	–	$<$0.10	0.014
CN	N=1–0	–	–	–	$<$0.30[c]	–
CN	N=2–1	–	–	–	$<$0.20[c]	0.055
CS	J=2–1	0.064	114.5	4.2	0.29(0.043)	0.014
CS	J=3–2	0.026	114.8	5.7	0.16(0.016)	0.0019
CS	J=5–4	–	–	–	$<$0.12	0.024
^{13}CS	J=3–2	–	–	–	$<$0.067	0.0060
SO	J_N=3_2–2_1	0.024	114.7	4.4	0.11(0.032)	0.0072
SO	J_N=4_3–3_2	0.017	114.2	5.1	0.093(0.022)	0.0056
HCO$^+$	J=1–0	0.11	114.2	5.2	0.62(0.063)	0.051
HCO$^+$	J=3–2	–	–	–	$<$0.19	0.050
H^{13}CO$^+$	J=1–0	0.0028	114.4	3.9	0.012(0.0080)	0.0026
DCO$^+$	J=2–1	–	–	–	$<$0.043	0.0040
HCN	J=1–0	0.023	117	11.0	0.27(0.098)	0.019
HCN	J=3–2	–	–	–	$<$0.30	0.13
HNC	J=1–0	–	–	–	$<$0.050	0.018
C_2H	$N(J,F)$=1($\frac{3}{2}$,2)–0($\frac{1}{2}$,1)	0.039	114.5	7.4	0.31(0.032)	0.012
C_2H	$N(J,F)$=1($\frac{3}{2}$,1)–0($\frac{1}{2}$,0)	0.029	114.7	5.5	0.17(0.028)	0.012
C_2H	N=1–0	–	–	–	0.77[c]	–
o-H_2CO	$J_{K_{\rm p},K_{\rm o}}$=$2_{1,2}$–$1_{1,1}$	0.035	115.5	5.8	0.22(0.039)	0.0047
o-H_2CO	$J_{K_{\rm p},K_{\rm o}}$=$2_{1,1}$–$1_{1,0}$	0.022	115.3	6.5	0.16(0.030)	0.0072
p-H_2CO	$J_{K_{\rm p},K_{\rm o}}$=$2_{0,2}$–$1_{0,1}$	0.026	114.5	5.8	0.16(0.034)	0.0042
HC_3N	J=16–15	–	–	–	$<$0.093	0.0072
CH_3OH, c-C_3H_2	$\nu\approx$145.1 GHz	–	–	–	$<$0.036	0.0038

[a] The numbers in brackets are 2σ noise fluctuations.
[b] 2σ rms noise.
[c] Total intensity. Not observed hfs components have been accounted for by assuming LTE.

various species (i.e., abundances relative to that of molecular hydrogen). We defined the cloud-boundary as the extent of the CO(J=1–0) line emission. As a measure of the hydrogen content inside the CO boundary we used the virial mass. Moreover, we assumed that hydrogen is in fully molecular form. The total number of a trace molecule 'mol' in a cloud was calculated as the integral of the column density over the cloud. We used the same approximation for the radial distribution of the column density as was used above for the emitted line intensity, i.e., a Gaussian with a FWHM size of $S_{\rm mol}$. If S is the FWHM size of the cloud, we define the radius of a cloud as:

$$R = 0.8 \times S \quad (2)$$

The choice of the factor 0.8 (rather than the more intuitive 0.5) is motivated by: (1) Solomon et al. (1987) find in their work on Galactic clouds that $R\approx0.82\times S$; (2) an estimate of the observational effects on the relation between the equivalent radius

Table 10. Integrated intensity ratios

Molecule(s)	Transitions	N159W	N159S	N160	30Dor-10	30Dor-27	N27
CO	2–1/1–0	1.0[a]	0.70	–	1.2[b]	0.82[b]	0.96
CO	3–2/1–0	1.1[b]	0.60	–	2.1[b]	0.97[b]	0.75
^{13}CO	2–1/1–0	1.5[a]	1.0	1.9	2.6[b]	1.2[b]	1.2[d]
C^{18}O	2–1/1–0	1.8[c]	–	–	–	–	–
C^{17}O	2–1/1–0	2.7[c]	–	–	–	–	–
CN	1–0/2–1	2.4	–	–	–	–	–
CS	2–1/3–2	1.2	4.5	1.3	1.4	2.4	2.4
CS	2–1/5–4	3.4	–	5.4	3.6	–	>4.6
^{13}CS	2–1/3–2	0.70	–	–	–	–	–
C^{34}S	2–1/3–2	0.96	–	–	–	–	–
SO	3_2–2_1/4_3–3_2	1.1	2.1	–	–	<2.8	1.6
SO	3_2–2_1/6_5–5_4	3.0	–	–	–	–	–
SO	4_3–3_2/6_5–5_4	2.7	–	3.3	4.0	–	–
HCO$^+$	1–0/3–2	4.0	–	4.4	4.0	–	>4.0
HCN	1–0/3–2	>3.0	–	–	–	–	>2.0
H_2CO	$2_{1,2}$–$1_{1,1}$/$2_{1,1}$–$1_{1,0}$	1.5	1.2	1.1	1.9	1.8	1.5
H_2CO	($2_{1,2}$–$1_{1,1}$ + $2_{1,1}$–$1_{1,0}$)/$2_{0,2}$–$1_{0,1}$	3.0	2.6	2.2	3.3	–	2.3
H_2CO	$2_{1,1}$–$1_{1,0}$/$3_{1,2}$–$2_{1,1}$	2.1	–	–	>4.2	–	–
H_2CO	$2_{0,2}$–$1_{0,1}$/$3_{0,3}$–$2_{0,2}$	1.9	–	–	2.4	–	–
H_2CO	$2_{1,2}$–$1_{1,1}$/$3_{1,3}$–$2_{1,2}$	3.2	–	–	–	–	–
H_2CO	$3_{0,3}$–$2_{0,2}$/$3_{2,2}$–$2_{2,1}$	9.2±2.0	–	–	–	–	–
C_3H_2	$2_{1,2}$–$1_{0,1}$/$3_{1,2}$–$2_{2,1}$	6.3	–	–	–	–	–
C_3H_2	$2_{1,2}$–$1_{0,1}$/$4_{1,4}$–$3_{0,3}$	5.4	–	–	–	–	–
C_3H_2	$4_{1,4}$–$3_{0,3}$/$4_{0,4}$–$3_{1,3}$	1.2	–	–	–	–	–

The intensities have been corrected for large-scale beam-dilution.
Unless indicated, the total uncertainty in the ratios is estimated to be about ±30%.
[a] Data taken from Paper I.
[b] Data taken from Johansson et al.(1998).
[c] C^{17,18}O J=1–0 and J=2–1 data taken from Paper I and Heikkilä et al. (1998), respectively.
[d] For a source size of 45″. A source size of 70″ would yield a ratio of 1.5. Rubio et al. (1996) obtained 1.6.

(geometric mean of the semi-major axis and the semi-minor axis) of an ellipsoidal cloud approximated with a circular Gaussian intensity distribution gives R=(0.6–1)×S (Johansson et al. 1998); (3) a homogeneous spherical cloud with a constant density and R≈0.74×S contains the same mass as a cloud with a Gaussian column density distribution with a FWHM size of S. The use of an r^{-1} density-law for the spherical cloud and setting $N_{\rm H_2}$=2 R <n(H$_2$)> would give R≈0.82×S.

In the calculation of the virial mass, we assume a power-law (r^{-1}; r is the distance from the cloud centre) for the radial distribution of the gas density in a cloud. A constant gas density throughout the cloud would result in a virial mass that is 1.11 times higher than obtained from Eq. (3). The choice of an r^{-1} law rather than a constant gas density is motivated by studies of the radial density distribution in Galactic clouds (see e.g. MacLaren et al. 1988). Note that we use the r^{-1} law only in the calculation of the virial mass. Thus, this is not in conflict with the estimation of the molecular column densities with the MEP approach where the model cloud has a constant density. The virial mass [$M_{\rm vir}$ in units of M$_\odot$] corrected for the helium content by a factor of 1.36, the total number of hydrogen molecules [$\mathcal{N}_{\rm H_2}$], the total number of trace molecules and the fractional abundance of species 'mol' [$\mathcal{N}_{\rm mol}$, $X_{\rm mol}$], the mean gas density [$< n({\rm H_2}) >$ in cm^{-3}] of a cloud, and a measure of the column density of H$_2$ [$N_{\rm H_2}$ in cm^{-2}] along a line through the cloud centre can then be written as:

$$M_{\rm vir} = 151\, S_{\rm CO}\, \Delta v^2 \quad (3)$$

$$\mathcal{N}_{\rm H_2} = \frac{M_{\rm vir}}{1.36\, m_{\rm H_2}} = 6.60 \times 10^{58}\, S_{\rm CO}\, \Delta v^2 \quad (4)$$

$$\mathcal{N}_{\rm mol} = 1.08 \times 10^{37}\, S_{\rm mol}^2\, N_{\rm mol} \quad (5)$$

Table 11. Integrated intensity ratios, continued

Molecule(s)	Transitions	N159W	N159S	N160	30Dor-10	30Dor-27	N27
CO/^{13}CO	1–0/1–0	5.5	9.7	6.3	18	7.3	12
HCO$^+$/H^{13}CO$^+$	1–0/1–0	46	–	–	41±25	–	51±36
CS/^{13}CS	2–1/2–1	41	–	–	–	–	–
CS/^{13}CS	3–2/3–2	25	–	–	–	–	>2.4
CS/C^{34}S	2–1/2–1	19	–	–	–	–	–
CS/C^{34}S	3–2/3–2	16	–	–	–	–	–
SO/^{34}SO	3_2–2_1/3_2–2_1	>5.5	–	–	–	–	–
SO/^{34}SO	4_3–3_2/4_3–3_2	>12	–	>1.0	–	–	–
^{13}CO/HCO$^+$	1–0/1–0	1.1	4.6	0.61	0.26	1.0	0.94
CO/HCO$^+$	1–0/1–0	6.1	45	3.8	4.9	7.6	11
CO/C$_2$H[a]	1–0/1–0	9.6	40	7.9	8.8	4.8	8.8
HCN/HNC	1–0/1–0	3.1	3.6	–	4.4	–	>4.6
CN/HCN[a]	1–0/1–0	1.0	<0.84	0.62	1.2	<0.71	<0.84
CN/CS[a]	1–0/2–1	1.4	<0.40	1.6	1.8	<0.53	<0.89
SO/CS	3_2–2_1/2–1	0.42	0.23	–	–	–	0.38
SO/CS	4_3–3_2/3–2	0.45	0.49	0.71	0.31	0.36	0.56
SO/CS	6_5–5_4/5–4	0.49	–	0.92	0.20	–	–
SO/H$_2$S	4_3–3_2/$1_{1,0}$–$1_{0,1}$	1.1	–	–	–	–	–

The intensities have been corrected for large-scale beam-dilution.
Unless indicated, the total uncertainty in the ratios is estimated to be about ±30%.
[a] In the C$_2$H and CN N=1–0 lines the hyperfine structure has been accounted for by assuming LTE.

Table 12. Hyperfine and fine structure line ratios in N159W

Molecule	Transitions	Observed ratio	LTE ratio
CN	$1(\frac{1}{2},\frac{3}{2})$– $0(\frac{1}{2},\frac{3}{2})$/$1(\frac{1}{2},\frac{3}{2})$– $0(\frac{3}{2},\frac{1}{2})$	1.46	1.25
CN	$1(\frac{3}{2},\frac{3}{2})$– $0(\frac{1}{2},\frac{3}{2})$/$1(\frac{3}{2},\frac{1}{2})$– $0(\frac{1}{2},\frac{1}{2})$	1.19	1.00
CN	$1(\frac{3}{2},\frac{3}{2})$– $0(\frac{1}{2},\frac{1}{2})$/$1(\frac{3}{2},\frac{3}{2})$– $0(\frac{1}{2},\frac{3}{2})$	0.76	1.25
CN	$1(\frac{3}{2},\frac{5}{2})$– $0(\frac{1}{2},\frac{3}{2})$/$1(\frac{3}{2},\frac{3}{2})$– $0(\frac{1}{2},\frac{1}{2})$	3.17	2.70
CN	$1(\frac{3}{2},\frac{3}{2})$– $0(\frac{1}{2},\frac{1}{2})$/$1(\frac{3}{2},\frac{1}{2})$– $0(\frac{1}{2},\frac{1}{2})$	0.90	1.00
CN	$1(\frac{3}{2},\frac{5}{2})$– $0(\frac{1}{2},\frac{3}{2})$/$1(\frac{3}{2},\frac{1}{2})$– $0(\frac{1}{2},\frac{1}{2})$	2.88	3.375
CN	$1(\frac{3}{2})$–$0(\frac{1}{2})$/ $1(\frac{1}{2})$–$0(\frac{1}{2})$	4.1	2.0
C$_2$H	$1(\frac{1}{2},1)$– $0(\frac{1}{2},1)$/$1(\frac{1}{2},0)$– $0(\frac{1}{2},1)$	2.38	2.49
C$_2$H	$1(\frac{3}{2},2)$– $0(\frac{1}{2},1)$/$1(\frac{3}{2},1)$– $0(\frac{1}{2},0)$	1.74	2.01
C$_2$H	$1(\frac{3}{2},2)$– $0(\frac{1}{2},1)$/$1(\frac{1}{2},1)$– $0(\frac{1}{2},1)$	2.07	2.01
C$_2$H	$1(\frac{3}{2},1)$– $0(\frac{1}{2},0)$/$1(\frac{1}{2},1)$– $0(\frac{1}{2},1)$	1.19	1.00
C$_2$H	$1(\frac{3}{2},1)$– $0(\frac{1}{2},0)$+$1(\frac{3}{2},2)$– $0(\frac{1}{2},1)$/ $1(\frac{1}{2},1)$– $0(\frac{1}{2},1)$+$1(\frac{1}{2},0)$– $0(\frac{1}{2},1)$	2.30	2.15

The quantum number notation is $N(J,F)$.

$$X_{\rm mol} = \frac{\mathcal{N}_{\rm mol}}{\mathcal{N}_{\rm H_2}} = 1.64\times10^{-22}\,\frac{S^2_{\rm mol}\,N_{\rm mol}}{S_{\rm CO}\,\Delta v^2} \quad (6)$$

$$\langle n({\rm H_2})\rangle = \frac{3\mathcal{N}_{\rm H_2}}{4\pi R^3} = 1047\,\frac{\Delta v^2}{S^2_{\rm CO}} \quad (7)$$

$$N_{\rm H_2} = 2R\,\langle n({\rm H_2})\rangle = 5.17\times10^{21}\,\frac{\Delta v^2}{S_{\rm CO}} \quad (8)$$

where $S_{\rm CO}$ and $S_{\rm mol}$ are the de-convolved FWHM sizes (in pc) of the cloud as measured by the CO(J=1–0) line and a line of a molecule 'mol', respectively, Δv (km s^{-1}) is the FWHM line-width of the average of CO(J=1–0) spectra observed within the FWHM size, and $m_{\rm H_2}$ is the mass of the hydrogen molecule (3.34×10^{-27} kg). In Table 13 we have also given the visual

Table 13. Adopted cloud parameters

Cloud	$n(H_2)$ [cm^{-3}]	$< n(H_2) >$[a] [cm^{-3}]	T_{kin} [K]	Θ_{mol}[b] [″]	Θ_{CO}[c] [″]	S[d] [pc]	M_{vir}[e] [10^5 $M_\odot$]	Δv_{CO}[f] km s^{-1}	N_{H_2}[g] [$10^{22} cm^{-2}$]	A_V[h] mag
N159W	3×10^5	130	25	40	65	16.7	0.90	6.0	1.1	2.9
N159S	1×10^5	160	10	70	85	21.8	2.4	8.5	1.7	4.5
N160	5×10^5	210	20	30	40	10.3	0.34	4.7	1.1	2.9
30Dor-10	1×10^5	330	50	50	78	20.1	3.8	11.2	3.2	8.6
30Dor-27	5×10^4	150	15	30	40	10.4	0.24	4.0	0.78	2.1
N27	1×10^5	110	15	45	70	21.4	1.5	6.8	1.1	1.0

[a] The average gas density from the virial mass, see Eq. (7).
[b] The angular cloud size as defined by the FWHM extent of the line emission from molecules other than ^{12}CO and HCO^+.
[c] The angular cloud size as defined by the FWHM extent of the $^{12}CO(J$=1–0) line emission.
[d] The linear cloud size as defined by the FWHM extent of the $^{12}CO(J$=1–0) line emission. For the clouds in the LMC, see Johansson et al. (1998). The distances to the LMC and the SMC were taken as 53 and 63 kpc, respectively.
[e] The virial mass, see Eq. (3).
[f] LMC data from Johansson et al. (1998). The line-widths refer to a spectrum averaged over the source.
[g] A measure of the column density of H_2 through the cloud centre, see Eq. (8).
[h] The visual extinction as estimated from N_{H_2}.

Table 14. Kinetic temperatures (T_{kin})

Tracer	N159W	N159S	N160	30Dor-10	30Dor-27	N27
^{12}CO[a]	>17	11–21	–	>30	>12	>10
^{13}CO[a]	8–17	6–11	11–23	15–60	7–13	7–15
$C^{18}O$[a]	10–21	–	–	–	–	–
$C^{17}O$[a]	17–69	–	–	–	–	–
HCO^+/DCO^+[b]	25±2	–	–	–	–	>21
HCO^+/DCO^+[c]	10–24	–	–	–	–	–
H_2CO	30±3	–	–	–	–	–
CH_3CCH	<31	–	–	–	–	–
Brightness temperature of ^{12}CO lines	>10	>5	>6	>2	>3	>3
Upper energy levels of detected transitions	<68	<33	<51	<51	<33	<33
LTE excitation temperature, ^{12}CO, assumed optically thick	>14	>10	>10	>5	>7	>6
LTE excitation temperature, ^{13}CO, assumed optically thin	11	8	11	24	9	9
LTE excitation temperature, $C^{18}O$, assumed optically thin	13	–	–	–	–	–
LTE excitation temperature, $C^{17}O$, assumed optically thin	27	–	–	–	–	–
LTE excitation temperatures, other molecules	5–15	3–5	5–10	5–10	4–6	3–5

The temperatures are expressed in Kelvin [K].
[a] Calculated using the MEP approach with $n(H_2)$=3×10^4 cm^{-3}.
[b] Using a simplistic approach to deuterium fractionation, see Heikkilä et al. (1997a).
[c] Using results of a chemical model for a Galactic dark cloud by Millar et al. (1989), see Heikkilä et al. (1997a).

Table 15. Number densities ($n(H_2)$)

Tracer	N159W	N159S	N160	30Dor-10	30Dor-27	N27
CS, ^{13}CS, $C^{34}S$	(3–9)×10^5	<2×10^5	(2–15)×10^5	(1–3)×10^5	(6–250)×10^3	(7–300)×10^3
SO	(2.5–8)×10^5	(3–50)×10^4	(2.5–20)×10^5	(7–30)×10^4	>2×10^4	(5–100)×10^4
HCO^+	(4–20)×10^4	–	(4–30)×10^4	(2–15)×10^4	–	<4×10^5
HCN	<1.5×10^6	–	–	–	–	<8×10^6
H_2CO	(1.5–20)×10^5	>5×10^4	>1×10^5	<4×10^5	<5.5×10^5	(1–300)×10^4

The number densities are expressed in cm^{-3}.

Table 16. Molecular column densities from MEP analysis

Molecule	N159W	N159S	N160	30Dor-10	30Dor-27	N27
CO	1.6(17)	9.3(16)	5.4(16)	5.4(16)	3.2(16)	2.0(16)
^{13}CO	2.0(16)	5.7(15)	6.2(15)	3.6(15)	2.4(15)	1.4(15)
C^{18}O	5.4(14)[a]	<1.8(14)[a]	–	<8.1(13)	–	<5.8(13)[a]
C^{17}O	3.4(14)[a]	–	–	–	–	<1.8(13)
CN	2.5(13)	<5.5(12)	1.6(13)	1.4(13)	<6.8(12)	<4.0(12)
CS	2.3(13)	1.0(13)	7.7(12)	9.4(12)	1.7(13)	3.6(12)
^{13}CS	5.5(11)	–	–	–	–	–
C^{34}S	9.6(11)	–	–	–	–	–
SO	2.3(13)	7.8(12)	1.3(13)	5.4(12)	1.5(13)	4.1(12)
HCO$^+$	8.6(12)	1.5(12)	5.3(12)	4.3(12)	3.3(12)	1.5(12)
H^{13}CO$^+$	2.6(11)	–	–	1.2(11)	–	2.8(10)
DCO$^+$	9.1(10)[b]	–	–	–	–	<7.8(10)
HCN	1.1(13)	5.4(12)	8.7(12)	6.1(12)	1.4(13)	3.2(12)
HNC	3.5(12)	1.5(12)	–	1.4(12)	–	<6.9(11)
C_2H	2.7(14)	3.4(13)	1.4(14)	9.2(13)	9.5(13)	4.1(13)
para-H_2CO	5.4(12)	6.7(11)	3.4(12)	2.8(12)	–	1.1(12)
ortho-H_2CO	9.9(12)	4.3(12)	8.5(12)	6.1(12)	7.0(12)	2.6(12)
H_2CO	1.5(13)	5.0(12)	1.2(13)	8.9(12)	9.3(12)[c]	3.7(12)

$A(B)$ denotes $A \times 10^B$ [cm^{-2}].
[a] Data taken from Heikkilä et al. (1998).
[b] Data taken from Heikkilä et al. (1997a).
[c] Assuming an ortho/para ratio of 3.

extinction[4] (A_V) that corresponds to the column density of hydrogen nuclei N_H=2 N_{H_2}.

The resulting molecular abundances are collected in Table 18. Abundance ratios of isotopomers and other molecule pairs of interest are given in Table 19. Finally, Table 20 shows the abundances in the different clouds relative to the abundances derived for N159W (our 'reference cloud'): X_{mol}(N159W)/X_{mol}(source).

5. Discussion

Observationally, estimates of various physical and chemical quantities of an interstellar gas-cloud are averages over the spatial size-scales defined by the linear resolution of the antenna and, provided that optical depth effects can be accounted for, over the extent of the cloud along the line-of-sight. The resolution of the present observations is 10–15 pc in the λ=3 mm band, and 5–10 pc in the λ=2 and 1.3 mm bands, i.e. comparable to the extents of the studied clouds when the boundary is defined by the CO line emission (10–20 pc). Thus, in our study, the derived quantities should be seen as reflecting global averages for the individual clouds. The molecular line emission collected by the telescope consists of a conglomerate emerging from different, by the telescope non-resolved, regions with various physical and chemical properties. Accordingly, the accuracy in the determination of physical and chemical parameters is, besides instrumental and modelling uncertainties, also limited by their expected spatial variation, i.e. gradients. In Galactic star-forming regions it has become evident that the chemical properties of the gas can change on very small spatial scales (e.g. Johansson et al. 1984; Blake et al. 1987; Helmich & van Dishoeck 1997; Ungerechts et al. 1997; Nummelin et al. 1998). If the goal, as is the case in the present work, is to estimate *average* cloud properties, the uncertainties do not necessarily increase with decreasing spatial resolution, but are more determined by gradients present in the observed region. In this sense, if the parameters show rapid spatial variations, observationally derived parameters can actually suffer from larger errors when observed with a high spatial resolution than investigations with a lower spatial resolution, which probe more the average properties of the cloud. In particular, this is true if the line emission is less saturated in the latter case. Hence, it may be that, despite the lower spatial resolution in the observations, the quantities, seen as cloud averages, derived for the Magellanic Clouds are more accurate than those derived for Galactic clouds.

5.1. Physical state

5.1.1. Gas temperature

Johansson et al. (1998) found that gas temperatures estimated from CO line data for a sample of LMC clouds seem to mirror the environment of the clouds: regions showing vigorous star-formation activity tend to be warmer. This is reasonable since in

[4] We scaled the Galactic A_V/E(B-V) and N_H/E(B-V) relations [≈3.1 and 5.8×10^{21} cm^{-2} mag^{-1}, respectively, see Bohlin et al. (1978)] to the conditions appropriate for the Magellanic Clouds: A_V/E(B-V)=3.1 in the LMC and 2.7 in the SMC; N_H/E(B-V) was taken to be four times higher in the LMC and ten times higher in the SMC than in the Galaxy (Koornneef 1982; Bouchet et al. 1985).

Table 17. Molecular column densities and excitation temperatures from LTE analysis

Column density [cm^{-2}] Molecule	N159W	N159S	N160	30Dor-10	30Dor-27	N27
CO	1.4(17)	8.7(16)	5.6(16)	13(17)	2.8(16)	2.5(16)
^{13}CO	1.5(16)	5.8(15)	5.8(15)	2.4(15)	2.5(15)	1.4(15)
CN	4.6(13)	<5.7(12)[a]	2.0(13)[a]	1.7(13)[a]	<6.3(12)[a]	<6.1(12)[a]
CS	1.9(13)	1.1(13)[a]	8.8(12)	5.9(12)	1.5(13)	3.5(12)[a]
^{13}CS	6.3(11)	–	–	–	–	–
C^{34}S	1.1(12)	–	–	–	–	–
SO	2.3(13)	1.1(13)[a]	1.5(13)	4.3(12)[a]	8.5(12)	4.6(12)[a]
HCO^+	1.4(13)	2.2(12)	8.6(12)	6.6(12)	3.1(12)[a]	1.9(12)[a]
$H^{13}CO^+$	3.4(11)[a]	–	–	1.9(11)[a]	–	3.9(10)[a]
DCO^+	1.5(11)[a,e]	–	–	–	–	<9.0(10)[a]
HCN	1.2(13)[a]	2.1(12)[a]	1.0(13)[a]	4.8(12)[a]	3.7(12)[a]	1.4(12)[a]
HNC	4.7(12)[a]	7.0(11)[a]	–	1.3(12)[a]	–	<3.7(11)[a]
C_2H	2.7(14)[b]	6.6(13)	1.3(14)[b]	1.2(14)[b]	1.2(14)[b]	6.1(13)[b]
para-H_2CO	4.6(12)	1.6(12)[a]	5.6(12)[a]	2.3(12)	–	9.8(11)[a]
ortho-H_2CO	1.6(13)	3.4(12)[a]	1.1(13)[a]	1.2(13)	3.4(12)[a]	2.0(12)[a]
H_2CO	2.0(13)	4.9(12)[a]	1.7(13)[a]	1.4(13)	4.5(13)[a,c]	3.0(12)[a]
ortho-H_2S	6.4(12)[a]	–	–	–	–	–
H_2S	8.5(12)[a,c]	–	–	–	–	–
para-c-C_3H_2	6.3(12)[d]	–	–	–	–	–
ortho-c-C_3H_2	4.5(12)	–	–	–	–	–
c-C_3H_2	1.0(13)	–	–	–	–	–
CH_3OH A-sym.	7.9(12)[b]	–	–	–	–	–
CH_3OH E-sym.	6.7(12)[b]	–	–	–	–	–
CH_3OH	1.5(13)[b]	–	–	–	–	–
CH_3CCH	3.0(12)[b]	–	–	–	–	–
HC_3N	<2.5(12)[a]	–	–	–	–	–
HDO	<8.7(14)[b]	–	–	–	–	–
OCS	<1.1(14)[b]	–	–	–	–	–
SO_2	<4.8(12)[a]	–	–	–	–	–
H_2CS	<4.6(12)[a,c]	–	–	–	–	–
Excitation temperature [K] Molecule	N159W	N159S	N160	30Dor-10	30Dor-27	N27
^{13}CO	11.0	7.8	14.0	23.6	8.9	8.8
CN	4.3	–	–	–	–	–
CS	9.4	3.0	8.1	9.4	4.1	4.0
^{13}CS	14.8	–	–	–	–	–
C^{34}S	9.0	–	–	–	–	–
SO	10.0	4.9	9.2	10.0	10.0	6.0
HCO^+	6.0	–	5.8	6.0	–	–
para-H_2CO	7.2	–	–	6.2	–	–
ortho-H_2CO	5.4	–	–	4.1	–	–
ortho-c-C_3H_2	4.2	–	–	–	–	–

$A(B)$ denotes $A \times 10^B$.
[a] T_{ex}has been assumed: N159W, N160 and 30Dor-10 (5 K); N159S (4 K); 30Dor-27 and N27 (5 K).
[b] For species with an electric dipole moment <1 Debye, T_{ex}=10 K was used.
[c] Assuming an ortho/para ratio of 3.
[d] The same T_{ex} as for o-C_3H_2 was used.
[e] Data taken from Heikkilä et al. (1997a).

Table 18. Molecular fractional abundances

Molecule	N159W	N159S	N160	30Dor-10	30Dor-27	N27
CO	1.2(-5)	4.6(-6)	4.2(-6)	1.4(-6)	3.4(-6)	1.5(-6)
^{13}CO	5.8(-7)	1.9(-7)	2.7(-7)	3.9(-8)	1.5(-7)	4.3(-8)
CN	7.2(-10)	<1.8(-10)	7.1(-10)	1.5(-10)	<4.1(-10)	<1.3(-10)
CS	6.6(-10)	3.4(-10)	3.4(-10)	1.0(-10)	1.0(-9)	1.1(-10)
SO	6.6(-10)	2.6(-10)	5.7(-10)	5.8(-11)	9.0(-10)	1.3(-10)
HCO^+	2.5(-10)	5.1(-11)	2.3(-10)	4.6(-11)	2.0(-10)	4.6(-11)
HCN	3.2(-10)	1.8(-10)	3.8(-10)	6.6(-11)	8.4(-10)	1.0(-10)
HNC	1.0(-10)	1.2(-10)	–	1.4(-11)	–	<2.2(-11)
C_2H	7.8(-9)	1.1(-9)	6.1(-9)	9.8(-10)	5.8(-9)	1.3(-9)
H_2CO	4.4(-10)	1.7(-10)	5.2(-10)	9.5(-11)	5.7(-10)	1.1(-10)
H_2S	2.5(-10)[a]	–	–	–	–	–
c-C_3H_2	3.1(-10)[a]	–	–	–	–	–
CH_3OH	4.3(-10)[a]	–	–	–	–	–
CH_3CCH	8.6(-12)[a]	–	–	–	–	–
HC_3N	<7.1(-11)[a]	–	–	–	–	–
HDO	<2.6(-8)[a]	–	–	–	–	–
OCS	<3.1(-9)[a]	–	–	–	–	–
SO_2	<1.5(-10)[a]	–	–	–	–	–
H_2CS	<1.4(-10)[a]	–	–	–	–	–

$A(B)$ denotes $A \times 10^B$.
Nominal values are given.
[a] LTE analysis.

Table 19. Abundance ratios

Molecule	N159W	N159S	N160	30Dor-10	30Dor-27	N27
CO/^{13}CO	21	24	16	38	23	35
CS/^{13}CS	41	–	–	–	–	–
CS/C^{34}S	24	–	–	–	–	–
HCO^+/$H^{13}CO^+$	33	–	–	35±21	–	40–90
HCO^+/DCO^+	94	–	–	–	–	>19
HCN/HNC	3.1	3.6	–	4.5	–	>4.6
CN/HCN	1.1	<1.0	1.9	1.5	<0.5	<1.2
SO/CS	1.0	0.78	1.7	0.58	0.87	1.1
CN/CS	2.2	<0.6	2.1	2.3	<0.4	<1.2
CS/HCO^+	2.6	6.6	1.4	2.2	0.52	2.4
C_2H/HCO^+	31	22	26	21	29	28
^{13}CO/HCO^+	2300	3800	1200	850	740	920
ortho-H_2CO/para-H_2CO	1.8	4.0	2.5	2.2	–	2.4
ortho-c-C_3H_2/para-c-C_3H_2	0.71±0.32[a]	–	–	–	–	–
CH_3OH A-sym./E-sym.	1.2[a]	–	–	–	–	–

Nominal values are given. Unless indicated, the estimated uncertainties (total 2σ) are about ±30%
[a] LTE analysis.

such areas FUV photons are abundant, a high number of cosmic-rays may be present, and stellar winds and shocks are likely common. The temperature estimates varied from ≈10 K for the quiescent cloud N159S (based on the HCO^+(J=1–0)/CO(J=1–0) line intensity ratio) to ≈50 K for the 30Dor-10 cloud which is centered at the 30Dor nebula. The dust temperature, as traced by 100/60 μm flux ratio, shows the same trend. Also a sample of molecular clouds in the SMC (Lequeux et al. 1994), in M 33 (Wilson et al. 1997), and our estimates of the temperature in N159S, N160 and N27 follow the same trend with respect to star-formation activity as described above.

The HCN/HNC abundance ratio possibly has a temperature dependence, with a ratio >1 indicating warm gas (e.g. Schilke et al. 1992). We see no correlation between the HCN/HNC ratio and the gas temperature in our sample, all clouds have ratios >3.

At a first sight, the estimated gas temperature in molecular clouds in the LMC and SMC, typically 20–30 K, appears surprisingly low considering the intense FUV radiation that is

Table 20. Abundances relative to N159W: $X_{\rm mol}$(N159W)/$X_{\rm mol}$(source)

Molecule	N159S	N160	30Dor-10	30Dor-27	N27	TMC-1[a]	L134N[b]
^{12}CO	2.2	2.4	7.1	2.9	4.4	0.21	0.15
^{13}CO	3.0	2.1	14.9	3.9	13.6	0.70[h]	0.51[h]
CN	>3.9	1.0	5.2	>1.8	>5.8	0.024	>0.24
CS	2.0	2.0	6.6	0.63	5.9	0.33[k]	0.66
SO	2.5	1.2	11.5	0.74	5.2	0.13	0.033
HCO^+	4.8	1.1	5.4	1.2	5.4	0.031	0.031
HCN	1.8	0.85	4.9	0.38	3.2	0.027	0.080
HNC	0.86	–	7.1	–	>4.8	0.013	0.017
C_2H	6.8	1.3	7.9	1.4	6.0	0.92[k]	>0.15
H_2CO	2.4	0.86	4.7	0.78	3.9	0.037	0.022
Average[j]	2.5[l]	1.3	7.5	1.3	6.2	0.16	0.19

Molecule	IC 63[c]	NGC 7023[d]	Orion Bar[e]	Orion[a] (Extended Ridge)	Sgr B2[a]	S138[f]	Translucent[g] clouds
^{12}CO	0.20	–	0.16	0.24	0.20	–	–
^{13}CO	0.74	0.29	–	0.81[h]	0.24[h]	–	–
CN	0.13	2.2	0.15	0.22	2.1	–	–
CS	0.35	1.9	0.037	0.26	0.22	0.14	0.10
SO	>0.66	–	0.093	>0.72	4.4	0.19	0.022
HCO^+	0.16	0.13	0.10	0.11	0.11	0.28	0.36
HCN	0.040	0.78	0.090	0.064	0.11	0.073	0.041
HNC	0.045	0.16	0.14	0.19	0.034	0.12	0.028
C_2H	2.2	5.2	5.2	1.5	–	–	–
H_2CO	0.44	–	0.094	0.026[i]	0.15	–	0.044
Average[j]	0.27	0.91[m]	0.10	0.24	0.93[n]	0.19	0.099

[a] Data taken from Table 4 in Blake et al. (1987).
[b] Data taken from Ohishi et al. (1992).
[c] Data taken from Table 1 in Jansen et al. (1995a).
[d] Data taken from Table 4 [pos. (-20″, 100″)] in Fuente et al. (1993). We set $N_{\rm H_2}$=0.5 $N_{\rm H}$.
[e] Data taken from Table 4 [pos. (20″, -20″)] in Jansen et al. (1995b).
[f] Data taken from Johansson et al. (1994).
[g] Averages from Turner (1996), Turner et al. (1997) and references therein.
[h] Calculated from CO using ^{12}CO/^{13}CO=70 in Orion, TMC-1 and L134N, and ^{12}CO/^{13}CO=25 in Sgr B2.
[i] Compact Ridge value used for Orion.
[j] ^{13}CO, CN, CS, SO, HCO^+, HCN, HNC, and H_2CO included.
[k] Data from Ohishi et al. (1992) would give 0.066 (CS) and 0.11 (C_2H), respectively.
[l] 2.1 if also HCO^+ is excluded.
[m] 0.34 if also CN and CS are excluded.
[n] 0.14 if also CN and SO are excluded.

present. However, this value represents a global average over an individual cloud and small-scale variations with hotter as well as colder areas are very likely present. Emission from the fine-structure line at λ=158 μm of ionised carbon (C^+) is spatially extended in the LMC (Mochizuki et al. 1994; Poglitsch et al. 1995; Israel et al. 1996). The upper level of this line has an energy corresponding to 91 K and hence traces warm gas. In order to probe such a warm gas component by molecular line emission, observations of transitions with higher upper level energies than those observed by us would be required. The line emissions observed by us likely emerge from the cores of the clouds. In addition, trace molecules may well be dissociated in the gas component traced by the C^+ line emission. Boreiko & Betz (1991) obtained upper limits to the intensity of the CO(J=9–8) line (upper level energy ≈250 K) emission in a few locations in the LMC.

Despite the lower metallicity and the lower dust-to-gas ratio in the SMC, our results for N159W and N27 suggest that the gas temperature is not strongly affected. In particular, the temperature does not seem to be higher in N27. This could be a signature of a less efficient photo-electric heating due to the lower dust abundance or a more efficient cooling by CO due to optically thinner lines in the SMC.

The higher temperature in 30Dor-10 could, besides being caused by the intense FUV radiation from numerous massive stars, also result from a higher cosmic-ray flux owing to the presence of several supernova remnants in this area (provided that cosmic-rays originate from supernovae). In addition, the

CO line luminosity (normalised with the cloud mass) is lower in this area, cf. the luminosity vs. mass relation in Johansson et al. (1998), implying a less efficient cooling by CO. However, this loss of cooling by CO is counteracted by an increased far-infrared (FIR) line emission from C^+ and O.

The dust temperature, as measured by the 100/60 μm flux ratio, appears to exceed the gas temperature in all the studied clouds. Moreover, the temperature of the dust and the gas seem to correlate with the intensity of radiation in the UV and FUV (as traced by Hα and C^+ line emission) in the observed regions. This suggests that the dust is heated by the absorption of FUV photons, while the gas is primarily heated by electrons injected into the gas by the photo-electric effect on dust grains. The density in the bulk of the molecular gas in our sample of clouds is probably not high enough to allow for an efficient heating of the gas by gas-grain collisions. For a cloud, with $T_{\rm gas}$=25 K and $T_{\rm dust}$=40 K, which is exposed to a FUV field equal to that in the local Galactic ISM, a gas density of $>$few$\times10^5$ cm^{-3} is needed in order for gas-grain collisions to contribute more to the gas heating than the photoelectric effect. Expressions for the heating rates were taken from Black (1987). The stronger FUV field and the lower dust-to-gas ratio in the Magellanic Clouds imply that an even higher gas density is required there. Israel et al. (1996) argued for a high efficiency ($\sim$1% of the incident FUV flux being converted into thermal motion of gas particles) for the photo-electric heating of the gas in photon-dominated regions (PDRs) in the N159 and the N160 regions. The grains are typically smaller [although very small grains appear to be underabundant, cf. Lequeux (1989) and Rodrigues et al. (1997)], and consequently the photoelectric heating is more efficient in the Magellanic Clouds compared to the Galaxy (e.g. Watson 1972). A detailed modelling of the temperature structure of a molecular gas-cloud which is subjected to the conditions prevailing in the Magellanic Clouds is beyond the scope of the present paper.

5.1.2. Gas density and cloud structure

The structure of molecular clouds in the LMC and the SMC appears to differ considerably from that of Galactic clouds: the degree of clumping (as traced by CO and other trace molecules) is higher (see below), the linear sizes (as traced by CO) are smaller (Johansson et al. 1998), the fraction containing PDR gas is higher (Israel et al. 1996), and the fraction of atomic gas is possibly higher (Lequeux et al. 1994) in the Magellanic Clouds.

The density estimates for the different clouds show, considering the uncertainties in the observational data and the model, no significant variation. This does not imply that gas of other densities, in particular lower (e.g. a dilute interclump medium), is not present, but rather that the abundance and the excitation of trace molecules are low in such areas. The obtained density estimates are all close to the critical densities for the various lines. Generally, in all clouds, 'high-density' tracers (such as CS, HCN,...) yield densities $\sim10^5$ cm^{-3} with an upper limit of a few$\times10^6$ cm^{-3}, while the CO data, using the temperature as indicated by other tracers, give a lower limit of few$\times10^3$ cm^{-3}. HCO^+ data is compatible with densities in between those obtained from CO and other molecules. This agrees with the HCO^+(J=1–0) line emission appearing to be spatially more extended than that of other high-density tracers and more similar to that of CO. Taken together, this may indicate the presence of several, medium dense, molecular gas components. Also very compact areas with a considerably higher density and temperature (e.g. 'hot cores') may be present, but they contribute very little to the total emitted line intensity.

When discussing the clumpiness of the molecular gas, we emphasize that the results apply only to gas seen in the line emission from trace molecules. The clumpiness of the hydrogen gas needs not to be equal to that of trace molecules. Also, due to varying excitation requirements, differences among the trace molecules may exist. A comparison between the number density estimates from the excitation calculations and the 'average' density obtained from the virial mass leads to small-scale volume-filling factors of typically $\sim10^{-3}$–10^{-1} for the studied clouds. Accordingly, the clouds appear to be very clumpy and porous. Comparing the brightness temperatures of the CO lines and the estimated kinetic temperature of the gas, we find area-filling factors $\sim$0.05–1; e.g., $\sim$0.5 in the N159W and $\sim$0.05 in 30Dor-10. A relatively high area-filling factor is compatible with a very low volume-filling factor if the medium is clumpy: the probability to see at least one clump along each line-of-sight is then high independent of the optical depth of the line emission. Judging from the *area-filling* factors, the molecular gas seems to be more clumpy in 30Dor-10 than in the rest of the sample. However, the low CO brightness temperature in 30Dor-10 more likely reflects a low optical depth for the CO line emission (i.e., a low column density and a high excitation), rather than a truly low area-filling factor of the hydrogen gas. Also, the volume-filling factor, which should better describe the true clumpiness of the hydrogen gas, is similar in all clouds, including 30Dor-10. Nevertheless, the violent environment of 30Dor-10 could, besides leading to a more rapid photodissociation of trace molecules resulting in lower abundances, also create a more fragmented and clumpy gas structure.

5.2. Chemical composition

5.2.1. General remarks

Here we discuss the chemical composition of our sample of clouds in terms of molecular abundances (relative to H_2) and abundance ratios. The discussion applies to the gas-volume contained inside the boundary defined by CO line emission. The estimate of the molecular hydrogen content, which is needed in the abundance estimation, is based on the assumption that the virial mass provides a measure of the 'true' gas mass within the CO boundary. Therefore, a possible contribution from atomic hydrogen to the total mass of the cloud is included. However, we cannot separate the contributions from the atomic and the molecular component. Hence our abundance estimates inside the CO boundary can be seen as lower limits, considering the

possibility of significant amounts of atomic gas in the interclump medium. On the other hand, any form of hydrogen outside the volume defined by CO is not accounted for. Pak et al. (1998) have detected FIR line emission from FUV excited H_2, along with weak CO(J=1–0) line emission, in areas outside the main clouds defined by CO line emission. In this respect, the abundances calculated by us likely provide an upper limit to the true global values. In our calculations we assume that hydrogen is in fully molecular form because we will compare molecular abundances not only within the Magellanic Clouds, but also with Galactic objects. In observational studies of Galactic clouds, the abundances usually are normalised with H_2. On the other hand, normalisation relative to the total number of hydrogen nuclei is often used in chemical models. In our case the conversion to the latter convention is made by reducing the abundance estimates for the LMC and SMC sources by a factor of two.

When comparing abundances for different clouds, a major source of possible systematic errors is the estimation of total mass and accordingly the molecular hydrogen content. Since we focus on relative, rather than absolute, differences between molecular abundances in different clouds, the assumption that the virial mass equals the true total mass can be relaxed to a linear relation. However, the degree of virial equilibrium may vary from cloud to cloud. Such a systematic effect could well be present in our sample, in particular in the violent region close to the 30Dor nebula. Against such an effect speaks the very similar size vs. line-width relations for the clouds identified in the 30Dor and the N159 areas (Johansson et al. 1998), suggesting these two areas to be virialised to the same degree. This is a statistical result, and accordingly individual clouds may deviate from this relation. Since the Magellanic Clouds interact mutually and with the Galaxy, as systems they are likely out of equilibrium. But again, individual molecular clouds in such a system may well be in equilibrium. Therefore, although the use of the virial mass as a measure of the total molecular hydrogen content of a cloud can be questioned, we believe that in our case this is the best procedure. Other methods, e.g. to normalise the column densities of 'non-^{12}CO' species with the ^{12}CO column density, or to use a ^{12}CO-to-H_2 conversion factor to determine the H_2 column density, would be even more problematic because the CO abundance and the conversion factor may vary within regions in the LMC and between the Galaxy, the LMC and the SMC.

Summarising, we believe that the results of our analysis concerning relative differences between the clouds are significant. In the following analysis, we have chosen N159W in the LMC to be our reference source, since the data-set is the largest and of the highest quality for this cloud.

5.2.2. Comparison with Galactic clouds

The Galaxy is a natural reference when interpreting observational results of extragalactic sources. Here we have compared the abundances in N159W with data collected from the literature for the following Galactic clouds: three molecular clouds associated with the formation of massive stars (the Orion (extended) ridge, Sgr B2, S138), two dark clouds (TMC-1, L134N) and three PDRs (IC 63, NGC 7023, the Orion Bar). In addition, we have compared with data for small translucent clouds. The abundance comparison with S138 is probably the most appropriate, since the abundances there were estimated from mapping observations. Accordingly, the abundances in S138 describe global averages similar to the abundances estimated for our LMC/SMC sample. As is evident from Table 20, in some cases substantial scatter is present in the abundance comparisons between N159W and the chosen Galactic clouds. This reflects the uncertainties in the abundance determinations superposed on the intrinsic differences in the cloud properties. Nevertheless, some clear trends are discernible. For example, if the following group of molecules with similar abundances are chosen: CS, CN, HCN, HNC, HCO^+, and H_2CO, their abundances are about 1×10^{-8} in Galactic dark clouds and a few$\times10^{-9}$ in massive star-forming regions. The small translucent clouds, depending on the extinction, show values in between these limits. On the other hand, a typical abundance in N159W is 5×10^{-10}. We find that the abundances in N159W are lower by about a factor of five relative to those in Galactic clouds associated with PDRs and the formation of massive stars, and about a factor of twenty relative to the abundances in Galactic dark clouds (see further Table 20). It is interesting to note that the PDR NGC 7023 possibly shows abundances which are comparable to those in N159W. Such low abundances probably mirror the strong FUV radiation in NGC 7023. Moreover, in this source an abundance gradient may be present; lower abundances are found closer to the ionising star, further demonstrating the effect of FUV radiation on molecular abundances (Fuente et al. 1993). For a similar effect in the LMC, when different clouds are compared, see Sect. 5.2.3. The observed metallicity in H II regions in the LMC is on the average 2.8 times lower than in Orion [data from Dennefeld (1989)]. Using the average of the elemental abundances in Orion, M17 and M8 [data from Peimbert et al. (1993)] the metallicity in the LMC is lower by a factor of 5.1. A combination of the low metallicity and higher photodissociation rates in the LMC most likely explains the molecular underabundances in N159W. This is in line with model predictions (Bel et al. 1986). Concerning possible effects of a varying H/H_2 ratio, see Sect. 5.2.6. Compared to Galactic clouds, besides the generally lower abundances, a remarkable feature concerning individual molecular species in the LMC/SMC is the, in a relative sense, high abundance of the ethynyl radical (C_2H), see Sect. 5.3.1.

5.2.3. Abundance variations within the Magellanic Clouds

Examining the clouds individually, the derived abundances for the various molecules show internal consistency in the sense that the majority of the molecular species in a particular cloud show similar underabundances relative to the corresponding species in N159W. When comparing the mean abundance (average of all observed species) in the various clouds in our sample, abundance variations are clearly discernible (cf. Table 20), although the sample is admittedly small. More specifically, two of the clouds: N27 and 30Dor-10, stand out by showing lower abun-

dances than the other clouds. The abundances in N27 and 30Dor-10 are on the average six and eight times lower, respectively, than in our reference cloud N159W. The remaining clouds show, within a factor of ≈2, identical abundances as N159W. If we, instead of abundances, compare the molecular column densities, we find that these are on the average 6.7 and 2.8 times lower in N27 and 30Dor-10, respectively, than in N159W. These three sources show very similar spatial extents (17–21 pc). The virial masses in N27 and 30Dor-10 are 1.6 and 4.4, respectively, times higher than in N159W. Thus, the suggested abundance differences between these three clouds appear not to be caused by possible uncertainties in the use of the virial mass as a measure of the H_2 content alone, but probably indicate a real deficit of molecules in N27 and 30Dor-10 as compared to N159W. Although the magnitude of the deficit in 30Dor-10 must be considered to be more uncertain than that in N27.

5.2.4. Effect of the metallicity

The lower molecular abundances found in N27 seem to mirror the metallicity difference between the SMC and the LMC. The molecular underabundances by a factor of ≈6 reflects well the deficits (by factors of 2–6) of the elements C, N, O, and S in H II regions in the SMC relative to H II regions in the LMC (Dennefeld 1989).

Chin et al. (1998) estimated molecular abundances in the molecular cloud associated with the H II region N12 (IRAS source LIRS 36) in the SMC. The abundances of detected species in their Table 2 are on the average 2.5 times lower than in N159W. Since Chin et al. used a somewhat different method to estimate abundances, we have re-calculated (using the MEP approach) the abundances in N12 with our method[5]; and confirmed their results by obtaining on the average ≈3 times lower abundances than in N159W. This indicates that the abundances in N12 actually are somewhat higher than in N27. In the molecular cloud associated with the H II region N66 in the SMC, the average of the ^{13}CO [observational data from Rubio et al. (1996)], HCO^+ and CS abundances is five times lower than in N159W[6].

Thus, although the data indicate variations in the molecular abundances in the SMC as well, we see a clear trend of underabundances relative to the LMC. We attribute this to the lower metallicity in the SMC.

5.2.5. Effect of the FUV radiation

Although the systematic errors in the abundance estimates may be more serious in 30Dor – due to its extreme environment – than in other regions in the LMC, we believe that the indicated underabundances in the 30Dor-10 cloud are significant (cf. Sects. 5.2.1 and 5.2.3). This is supported by the fact that the CO emission is substantially weaker in the 30Dor region, in comparison with other areas associated with prominent H II regions in the LMC (cf. Israel et al. 1993). It is tempting, provided that the elemental abundances in the LMC are relatively uniform on a global scale, to attribute the lower molecular abundances in the 30Dor-10 cloud to a more rapid photodissociation of molecules due to the stronger FUV radiation in this area. For example, the Hα flux (which reflects the intensity of UV radiation) is ≈7 times higher, and the FUV flux is ≈15 times higher, in 30Dor than in N159, cf. Sect. 2. This should lead to considerably higher photodissociation rates in the vicinity of the 30Dor nebula. The 30Dor-27 cloud, located at the outskirts of the 30Dor region and thus to a lesser extent exposed to intense radiation, seems to confirm this hypothesis by exhibiting abundances similar to those in the N159 area. However, this explanation is to some extent questioned by HCO^+ and CS data from other clouds in the 30Dor area (Johansson et al. 1998). These clouds also show weak molecular line emission and thus presumably low column densities as well as low abundances. The sizes of these clouds are similar to those in the present paper. Possibly, these clouds could have a lower gas density, leading to weaker excitation and less intense line emission.

We tried to find additional evidence for the effect of FUV radiation on molecular abundances by comparing CN/HCN intensity and abundance ratios in the different regions. One would expect the CN/HCN abundance ratio to reflect the strength of the radiation field, the abundance of CN being increased at the expense of HCN by photodissociation of the latter species. Fuente et al. (1993) found a clear correlation between the distance to the ionising star and the CN/HCN ratio in their study of the Galactic PDR NGC 7023. In fact, a weak trend of a higher CN/HCN abundance ratio in the more active clouds (N159W, N160 and 30Dor-10) is discernible in our data (cf. Table 19). The studies by Fuente et al. (1993) and Bergin et al. (1997b) suggest that also C_2H can be a tracer of the FUV radiation. We find a high C_2H abundance in clouds associated with vigorous star-formation activity, while the abundance in N159S–the most quiescent cloud in our sample–is significantly lower (see Sect. 5.3.1). This provides further support for the importance of the FUV radiation on the molecular abundances.

Another, although not dominating, possible cause for the low abundances in the 30Dor area could be that this region is intrinsically metal poorer than other regions in the LMC. Such an addition of metal poor gas could have resulted from a partial mixing of the ISM of the LMC and the SMC during a collision. The next most recent collision between the LMC and the SMC has been suggested to ultimately have led to the formation of 30Dor and its intense star-formation activity (Westerlund & Danzinger 1985).

Summarising, we believe that the main reason for the, by our data suggested, low molecular abundances in the centremost cloud in 30Dor is a more rapid photodissociation due to the intense FUV radiation present there.

[5] Here we used $\Theta_{\rm CO}$=40″, $\Theta_{\rm mol}$=30″ as estimated from the maps of Chin et al. (1998), Δv=3.6 km s^{-1} and $T_{\rm kin}$=20 K (Chin et al. 1998), and $n(\rm H_2)$=5×10^5 cm^{-3} [compatible with Chin et al. (1998)].

[6] In the calculation, we used $\Theta_{\rm CO}$=50″, $\Theta_{\rm mol}$=35″, and Δv=6.6 km s^{-1}. These source sizes were estimated by comparing the cloud radius quoted by Lequeux et al. (1994) and our FWHM size of N27, and applying the same scaling factor in N66.

5.2.6. Effect of the H/H_2 ratio

On a global scale, the relative amount of atomic vs. molecular hydrogen is higher in the Magellanic Clouds than in the Galaxy (e.g. Westerlund 1990, 1997). If this is the case inside 'molecular' clouds, in the interclump medium, as well, as has been suggested for the SMC by Lequeux et al. (1994), then the virial mass will over-estimate the molecular mass of a cloud. This would have consequences for the estimated molecular abundances. First, the abundance difference between the LMC and the Galaxy would be smaller. Second, the abundances in 30Dor-10 and N27 could be more similar to those in N159W, if the more intense radiation, causing a more rapid photodissociation of H_2 (30Dor-10), and the lower dust-to-gas ratio, implying a slower formation rate and a more rapid photodissociation of H_2 (N27), have increased the fraction of atomic gas inside these clouds as compared to the other clouds in our sample. Thus, a varying H/H_2 ratio in clouds in the LMC and SMC could offer an alternative explanation for the observed abundance differences. On the other hand, Chin et al. (1997, 1998) estimated the CO-H_2 conversion factors in a few clouds in the LMC and one cloud in the SMC to be close to the conversion factor determined for Galactic disc clouds. They interpreted this to imply that the interclump medium is predominantly in molecular form.

5.2.7. Effect of the relative abundances of atomic carbon and oxygen

Another characteristic of the Magellanic Clouds is the high oxygen-to-carbon ratio observed in H II regions (Dennefeld 1989; Garnett et al. 1995). Effects of this could be discernible in abundance ratios of certain molecules as a result of chemical reactions that are sensitive to the relative amount of atomic oxygen and carbon. One obvious candidate is the SO/CS ratio. Our data suggest the SO/CS abundance ratio to be close to one in the Magellanic Clouds. This is higher than generally found in star-forming clouds in the Galaxy (cf. data in Gottlieb et al. 1978; Minh et al. 1990, 1991; Ungerechts et al. 1997; Bergin et al. 1997a). Also the quantity O-C is important in determining the character of the chemistry since it describes the amount of oxygen that remains after the formation of CO molecules. In fact, in contrast with O/C, O-C decreases in the sequence the Galaxy, the LMC, the SMC. This is due to the decreasing elemental abundances in this sequence. Moreover, according to the dark cloud model by Millar & Herbst (1990), O_2 is the dominant carrier of oxygen in the SMC; whereas in the LMC oxygen is more evenly distributed among O, O_2 and CO. Hence, the amount of atomic oxygen may be very low in particular in molecular clouds in the SMC. This would imply that compared to the Galaxy, the destruction due to atomic oxygen may be less effective in the Magellanic Clouds (Millar & Herbst 1990). Such an effect may be a part of the explanation for the relatively high C_2H abundance estimated for clouds in the LMC and the SMC (see further Sect. 5.3.1). Furthermore, Chin et al. (1998) suggested, based on results from a revised version of the Millar & Herbst model, that the low observed CN/CS abundance ratio of <2 in N12 in the SMC, unless being caused by a low nitrogen abundance, possibly indicates the presence of fair amounts of molecular oxygen since it destroys CN but not CS. CN is also destroyed by atomic oxygen through the reaction CN + O $\rightarrow$ CO + N (e.g., Sternberg & Dalgarno 1995). In the three sources where we have detected CN, the average CN/CS abundance ratio is $\approx$2.2 (MEP analysis) and $\approx$2.6 (LTE), while in N159S, 30Dor-27 and N27, this ratio is <1.2.

5.2.8. Isotope ratios

Abundance ratios of isotopic substitutes are interesting e.g. as probes of stellar nucleosynthesis and the star-formation history. In addition, species that are vulnerable to chemical fractionation are useful as temperature probes and as tests of chemical models. For N159W, results of an LTE analysis were presented in Paper I.

Our estimate here, using the MEP approach, of the $^{12}C/^{13}C$ ratio (=36$\pm$11, average of CS and HCO^+ data) is close to those obtained in Paper I. The nominal carbon ratio obtained with the MEP approach is slightly lower than that with LTE. In 30Dor-10 our data give 35$\pm$21 for the $HCO^+/H^{13}CO^+$ abundance ratio. Using data from Chin et al. (1997), we estimate $HCO^+(J$=1–0$)/H^{13}CO^+(J$=1–0) abundance ratios of $\approx$45 and $\approx$33 in the N44BC and N113 clouds in the LMC, respectively. Hence, the $^{12}C/^{13}C$ ratio appears to be rather uniform among the studied clouds in the LMC. In the Galactic Centre, Galactic disc clouds and the outer Galaxy, the $^{12}C/^{13}C$ is $\approx$25, 40–100 and $>$200, respectively (Wilson & Rood 1994; Dahmen et al. 1995; Wouterloot & Brand 1996). The $^{12}C/^{13}C$ ratio may be slightly lower in the LMC than in the Galaxy (excluding the Galactic Centre), and thereby contradicts the notion that chemically young (low-metallicity) gas is poor in ^{13}C and has a high $^{12}C/^{13}C$ ratio (e.g. Wilson & Matteucci 1992). In the SMC the notoriously weak lines make the determination of isotopic ratios very difficult. Of the isotopomers that are useful for this purpose, and that are within reach using the present receivers at the SEST, we observed and marginally detected $H^{13}CO^+$. The nominal value of the resulting integrated intensity ($I_{\rm mb}$) from a Gaussian fit is 0.012 K km s^{-1}. Taking into account calibration and noise uncertainties, we find an $H^{12}CO^+/H^{13}CO^+$ abundance ratio of 52$\pm$36. A lower limit for this ratio can be estimated by treating the observed $H^{13}CO^+$ line as a non-detection; the upper limit for the intensity, calculated as described in Sect. 4.1, is then 0.014 K km s^{-1}, and consequently $H^{12}CO^+/H^{13}CO^+>44$. Based on these results, we estimate a gas-phase $^{12}C/^{13}C$ abundance ratio of 40–90 in N27. This value is, within the large uncertainties, in the same range as the values estimated for N159W and Galactic disc clouds. To corroborate the here presented results, estimates of the $^{12}C/^{13}C$ ratio using other probes (e.g. CS and HCN) in a larger cloud sample in the LMC and the SMC would be desirable. This because ^{13}C may to some extent fractionate in $H^{13}CO^+$ (Langer et al. 1984).

Based on $C^{32}S$ and $C^{34}S$ data, the $^{32}S/^{34}S$ ratio (=24$\pm$7) in N159W appears to be very similar to the Galactic. We tried to detect the $^{34}SO(J_N=3_2–2_1$ and $4_3–3_2)$ lines in N159W, in order to have another estimate of the $^{32}S/^{34}S$ ratio. The very tenta-

tive detection of the J_N=4$_3$–3$_2$ line would give ^{32}S/^{34}S≈22. In any case, the SO data implies ^{32}S/^{34}S>12. The, by Chin et al. (1998), tentatively detected C^{34}S(J=3–2) line in N12 in the SMC indicates a somewhat lower ^{32}S/^{34}S ratio there; our estimate using their data is ≈16. In the Galactic disc clouds, the ^{32}S/^{34}S abundance ratio is estimated to be close to 22 (Wilson & Rood 1994; Chin et al. 1996a).

The interstellar ^{18}O/^{17}O abundance ratio has been estimated to be ≈1.6 in the LMC. This is significantly lower than estimated for the Galactic ISM and centres of starburst galaxies. This was suggested to indicate that massive stars have contributed only little to the enrichment of the ISM in the LMC in the past (Heikkilä et al. 1998). The 30Dor region with its starburst character is a well suited target for investigating the influence of massive stars on the ^{18}O/^{17}O ratio. Our present data for 30Dor-10 show ^{13}CO/C^{18}O>38, which is similar to that in other clouds in the LMC (average ≈30), and possibly indicates a low ^{18}O/^{17}O ratio in this cloud as well. However, definite detections of line emission from both C^{18}O and C^{17}O in 30Dor-10 are needed to confirm this. High ^{13}CO/C^{18}O ratios have been observed in Galactic translucent and diffuse clouds. These ratios have been interpreted in terms of selective photodissociation (Gredel et al. 1994) and chemical fractionation (Liszt & Lucas 1998). Applying ^{12}CO/^{13}CO=20 (see Table 19) results in ^{16}O/^{18}O≈600 and ^{16}O/^{17}O≈950 in the LMC sample of Heikkilä et al. (1998). Compared to clouds in the inner Galaxy (Wilson & Rood 1994), the former ratio is about two times higher while the latter is about the same. This further emphasizes an underabundance of ^{18}O.

Accounting for fractionation, the observed DCN/HCN and DCO$^+$/HCO$^+$ ratios in LMC clouds are compatible with the D/H ratio in the Galactic interstellar medium (Chin et al. 1996b; Heikkilä et al. 1997a).

Due to the optical depth of the ^{12}CO lines, the column density estimates suffer from larger uncertainties than those of other species. The MEP code takes into account optical depth effects and suggests in all sources an optical depth of τ_{10}≈1 for the J=1–0 line, while it is higher for the J=2–1 and 3–2 lines. We used τ_{10}=1 when calculating the CO column density in the LTE approach by multiplying the optically thin value with $\tau/[1-\exp(-\tau)]$. The estimates of the ^{12}CO/^{13}CO ratio in the various clouds are lower than that of the elemental isotope ratio in N159W. A likely reason for the low ^{12}CO/^{13}CO ratio is chemical fractionation, which to be efficient needs a relatively cold gas and a high ^{13}C$^+$ abundance. Considering the observed strong and extended C$^+$ emission in the LMC, the latter criterion is conceivably fulfilled in the molecular clouds associated with star-formation regions in the LMC and the SMC, in particular, if they are highly clumpy. Assuming ^{12}C/^{13}C≈^{12}C$^+$/^{13}C$^+$ and ^{12}C/^{13}C≈40 would give ^{12}CO/^{13}CO=(^{12}C$^+$/^{13}C$^+$) ×exp $(-35/T_{\rm kin})$=7–17 for $T_{\rm kin}$=20–40 K. Thus, the observed ^{12}CO/^{13}CO abundance ratio (≈20) could be explained by chemical fractionation with some contribution from isotope selective photodissociation, which decreases the abundance of ^{13}CO relative to ^{12}CO. Also, depending on the relative amounts of carbon tied up in C$^+$ and CO, ^{12}C$^+$/^{13}C$^+$ may be higher than the total ^{12}C/^{13}C abundance ratio (Langer et al. 1984). A determination of the ^{12}C$^+$/^{13}C$^+$ abundance ratio using the FIR fine-structure lines would be useful. In N27 and 30Dor-10, ^{13}CO is even more underabundant than other molecules relative to N159W. The reason could be increased photodissociation rates.

5.3. Chemistry of selected species

5.3.1. C_2H and HCO^+

The prominent presence of C$^+$ in the Magellanic Clouds is expected to influence the resulting ion-molecule chemistry. We believe to see such signatures, most notably as a high abundance of the ethynyl radical (C_2H), but also as the abundance variations of C_2H and the formyl ion (HCO^+) with the environment, as well as the possibly large spatial extent of HCO^+ relative to other non-CO species.

It appears that, next to the CO isotopomers, C_2H is the most abundant trace molecule detected so far in the Magellanic Clouds (with the possible exceptions of CH and OH). Its average abundance, calculated using the MEP approach, in seven star-forming clouds in the LMC is 5×10^{-9}, which is similar to that in Galactic star-forming clouds. Here we included, besides clouds in our sample, data for three additional clouds[7] (N113, N44BC and N214DE) observed by Chin et al. (1997), but excluded the quiescent cloud N159S.

In the SMC source N27, the C_2H abundance is 1.3×10^{-9}. Using data from Chin et al. (1998), we obtained a C_2H abundance of $\approx5\times10^{-9}$ in N12 in the SMC. This suggests a high ethynyl abundance in the SMC as well.

In the gas-phase, ethynyl is formed via:

$$\mathrm{CH_x} \xrightarrow{\mathrm{C^+,H_2}} \mathrm{C_2H_2^+} \xrightarrow{\mathrm{e^-}} \mathrm{C_2H} \tag{9}$$

and from photodissociation of acetylene (C_2H_2):

$$\mathrm{h}\nu + \mathrm{C_2H_2} \rightarrow \mathrm{C_2H} + \mathrm{H} \tag{10}$$

while acetylene itself is formed in the gas-phase through:

$$\mathrm{CH_4} \xrightarrow{\mathrm{C^+}} \mathrm{C_2H_3^+} \xrightarrow{\mathrm{e^-}} \mathrm{C_2H_2} \tag{11}$$

Thus, an environment rich in C$^+$ and FUV photons, i.e. a PDR, provides an excellent platform for the production of large amounts of C_2H, and possibly also other simple hydrocarbons. Theoretical work by Mitchell (1984) suggests that the abundance of C_2H may also be increased in shocks. C_2H is destroyed

[7] The nominal C_2H abundances in N113, N44BC and N214DE are 7.9×10^{-9}, 4.1×10^{-9} and 2.5×10^{-9}, respectively. For these sources, we used $T_{\rm kin}$=20 K and $n(\mathrm{H_2})$= 5×10^5 cm^{-3}. The source sizes for N113, N44BC and N214DE were estimated from the ^{12}CO and ^{13}CO line emission maps presented in Chin et al. (1997), Kutner et al. (1997) and Heikkilä (1998). We arrived at the following FWHM source sizes as traced by ^{12}CO: 65″ (N113), 70″ (N44BC) and 95″ (N214DE). We used the extent of the ^{13}CO line emission as the source size for non-^{12}CO molecules, resulting in 55″ (N113), 50″ (N44BC) and 65″ (N214DE). The line-width of the ^{12}CO(J=1–0) line was taken from Chin et al. (1997).

mainly by photodissociation and in reactions with atomic oxygen (Mitchell et al. 1978). Since the abundance of free atomic oxygen is probably lower (see Sect. 5.2.7), in a relative sense, also the contribution of oxygen to the destruction of ethynyl will be lower in the Magellanic Clouds than in the Galaxy. This further helps to keep the C_2H abundance rather high in molecular clouds in the LMC and SMC. The electric dipole moment of C_2H is only 0.76 Debye. Therefore this molecule is relatively easily excited and may, in addition to the cloud cores or clumps, also trace more dilute gas located in the interclump medium and at clump surfaces where C^+ is common. The CO(J=1–0)/C_2H(N=1–0) line intensity ratio appears to correlate with the star-formation activity in a similar way as the CO(J=1–0)/HCO^+(J=1–0) ratio (see below): a significantly higher ratio is found in the quiescent cloud N159S than in the more actively star-forming clouds.

The abundance of HCO^+ correlates to some degree with the intensity of line emission from C^+ and with the star-formation activity. HCO^+ is, relative to other molecules, more underabundant in N159S and among the least underabundant in 30Dor-10 (N159W being the reference). This trend of a HCO^+ correlation with the star-formation activity is more clearly evident in the CO(J=1–0)/HCO^+(J=1–0) line intensity ratio determined for a larger sample of clouds in the LMC (Johansson et al. 1998). A more vivid star-formation activity gives rise to a higher FUV flux, and accordingly a more pronounced PDR character for the chemistry in clouds exposed to this radiation. We find a similar tendency of a decreasing CO/HCO^+ line intensity ratio with an increasing star-formation activity in the SMC: the ratio is lower in the very prominent star-formation regions N66 and N88 (≈11 and 16, respectively) than in the clouds with the strongest CO line emission N27 and N12 (≈21 and 25, respectively), and much lower than in the quiescent cloud SMC-B1 (≈74). The CO/HCO^+ line intensity ratio is ≈2 times higher while the CO/C^+ ratio is 1.4 times lower in N27 than in N159W. Here we used C^+ data for N27 from Israel & Maloney (1993). Of course a trend found in an intensity ratio suffers from uncertainties arising from the excitation of the involved lines. For example gas with a lower density would excite HCO^+ only weakly and possibly result in a high CO/HCO^+ ratio.

We made small maps of the HCO^+(J=1–0) line emission towards N27, N160, and 30Dor-10 in order to examine if the spatial extent of the HCO^+ line emission shows the same trend in these clouds as in N159W (see map in Paper I), i.e. being more similar to that of CO than other molecules. The signal-to-noise ratio in the individual positions is too poor to allow good contour maps to be produced. Instead, we have averaged the spectra in equidistant positions from the cloud-centre. The radial distributions of the integrated intensity in N27, N160 and 30Dor-10 are shown in Fig. 14. The resulting HCO^+ source size is in N27 ≈50″, in N160 ≈50″ and in 30Dor-10 ≈65″. Thus, the HCO^+(J=1–0) emission seems to be extended in these sources as well. However, better data are needed to corroborate this.

PDR chemistry, where the formation of HCO^+ mainly proceeds via reaction routes involving C^+, provides an attractive solution to the problem of the extended line-emission and the varying abundance of HCO^+ in the LMC. In the study by van der Werf et al. (1996), the observed different spatial distribution of CS and HCO^+ line emission in the Orion Bar, suggesting chemical stratification, was interpreted in terms of PDR chemistry. In regions shielded from FUV radiation, the principal formation processes of HCO^+ are

$$H_3^+ + CO \rightarrow HCO^+ + H_2 \quad (12)$$

$$HCS^+ + O \rightarrow HCO^+ + S \quad (13)$$

whereas the destruction proceeds via dissociative electron recombination and a reaction with H_2O, basically leading to CO production. In C^+ rich gas, e.g. in PDRs at cloud or clump surfaces, and in the interclump medium, HCO^+ is mainly formed via the reactions

$$C^+ + OH \rightarrow CO^+ + H \quad (14)$$

$$C^+ + O_2 \rightarrow CO^+ + O \quad (15)$$

$$CO^+ + H_2 \rightarrow HCO^+ + H \quad (16)$$

also

$$C^+ + H_2O \rightarrow HCO^+ + H \quad (17)$$

$$C + OH \rightarrow HCO^+ + e^- \quad (18)$$

$$O + CH \rightarrow HCO^+ + e^- \quad (19)$$

contribute to the formation of HCO^+, while its destruction is again largely governed by dissociative electron recombination, which mainly re-cycles HCO^+ into CO.

As can be seen from above, besides C^+, also the hydroxyl radical (OH) is important in the HCO^+ chemistry, directly in reactions (14,18), and indirectly by being involved in the formation of other simple oxygen-bearing molecules such as O_2, H_2O and CO. In PDRs, OH is produced in the endothermic reaction $O + H_2 \rightarrow OH + H$, and is thus temperature sensitive. Therefore, similar to C^+, the abundance of OH likely correlates with the intensity of FUV radiation, and emphasizes the coupling between HCO^+ and star-formation activity. Israel et al. (1982) estimated N(OH)≈8.7×10^{15} cm^{-2} in the N159 area. This value refers to observations by Whiteoak & Gardner (1976b) with a telescope-beam of $12\farcm4$ [which then encompasses the whole N159 complex of clouds (N159W, N159E and N159S) and part of N160] and an adopted source size of $3\farcm3$, and therefore is not directly comparable to our observations of line emission of other molecules at mm-wavelengths. Nevertheless, compared to other observed species the column density of OH appears to be high in the N159 area and may imply that this molecule is ubiquitous as a result of PDR chemistry. A tight correlation between the OH and HCO^+ column densities, N(HCO^+)/N(OH)=0.03–0.05, in Galactic clouds over a large range of visual extinction (A_V) has been inferred by Lucas & Liszt (1996). Assigning one third of the above quoted estimate of N(OH) in the N159 area to the N159W cloud (implying an OH abundance of about 8×10^{-8}) gives N(HCO^+)/N(OH)=0.003, which is an order of magnitude lower than in Galactic clouds. Interestingly, the ratio in N159W agrees better with the expectations resulting from a simple balancing of the rates [taken from

Millar et al. (1997)] of reaction (14) and dissociative electron recombination. By assuming that the abundances of electrons and C^+ are equal, we obtain $X(HCO^+)/X(OH) \approx 2.3 \times 10^{-5}\, T$. From the PDR model by Sternberg & Dalgarno (1995), we estimate $N(HCO^+)/N(OH)$ to be about 0.005 for $A_V < 4$ mag. On the other hand, the Millar et al. (1997) model for a Galactic dark cloud (A_V=10 mag) gives $N(HCO^+)/N(OH)$=0.02 (average of early time and steady-state results). The difference in the model results reflects the different character of the chemistry in regions with low/moderate and high extinction, respectively.

It would be useful to observe CH and OH lines with a high angular resolution to test the proposed PDR character of the chemistry in the Magellanic Clouds.

Further support for a PDR-type chemistry in N159W is provided by the low HC_3N/CN abundance ratio (<0.1). Low ratios are found in Galactic PDRs as well (Rodríguez-Franco et al. 1998). The formation of cyano acetylene (HC_3N) is chemically related to simple hydrocarbons, such as C_2H and C_2H_2. HC_3N is destroyed by FUV radiation and in reactions with C^+. On the other hand, the low observed nitrogen abundance observed in H II regions in the Magellanic Clouds may partially explain a low abundance of HC_3N.

5.3.2. Polyatomic molecules

Despite the conceivably unfavourable environment for the formation and survival of molecules in the Magellanic Clouds, a few moderately 'complex' (containing more than, say, three atoms) species have been detected. More specifically, thermal line emission from formaldehyde (H_2CO), cyclo-propenylidene (c-C_3H_2), methanol (CH_3OH), methyl acetylene (CH_3CCH), as well as tentatively from thio-formaldehyde (H_2CS) have been detected in the LMC. In the SMC, H_2CO and c-C_3H_2 have been detected (Chin et al. 1998; this paper). Detections of emission lines from interstellar methanol masers in the LMC have been reported by Sinclair et al. (1992), Ellingsen et al. (1994) and Beasley et al. (1996).

The methanol abundance in N159W is similar to that of other, less complex, molecules (cf. Table 18). This suggests that moderately complex molecules are not much more underabundant than more simple species in the ISM of the Magellanic Clouds. In Galactic clouds the abundance of methanol varies considerably depending on the cloud type: a few$\times 10^{-9}$ in dark clouds (Friberg et al. 1987), up to 10^{-6} in clouds associated with the formation of massive stars (Menten et al. 1988).

If grain chemistry provides a significant fraction of chemically saturated molecules, such as CH_3OH, H_2CO and H_2S, present in the gas-phase [as has been suggested for regions of high-mass star-formation in the Galaxy (e.g. Millar 1997)], then the involved surface processes appear to be fairly efficient. This considering the conditions that prevail in the Magellanic Clouds: strong FUV radiation, low dust content and probably, on the average, smaller and warmer grains; implying low sticking probabilities and a fast desorption.

5.4. Qualitative comparison with chemical models

Not many chemical models of molecular gas clouds with the conditions appropriate for the Magellanic Clouds have appeared in the literature. One reason for this has probably been the lack of observational data to compare with. A dark cloud model, allowing for the lower elemental abundances in the Magellanic clouds, was developed by Millar & Herbst (1990). More recently this model has been modified in order to take into account photo-processes, and been applied to observational data by Chin et al. (1996b, 1997, 1998). Effects of FUV radiation were considered in the models by Bel et al. (1986), Maloney & Black (1988), Lequeux et al. (1994) and Pak et al. (1998); the three latter studies deal mainly with H_2, CO and C^+, whereas Bel et al. considered a few other species as well. The chemical model by Bel et al. (1986) suggested that, in contrast to other molecules included in their study, the abundance of CH could become high even in the conditions that were taken to prevail in the Magellanic Clouds. This would result from C^+ being abundant due to the strong FUV radiation. In the dark cloud model by Millar & Herbst (1990), the abundance of C_2H does not differ very much between the Galaxy and the Magellanic Clouds. This is explained in terms of the lower abundance of free atomic oxygen in the Magellanic Clouds. Both these results of early attempts to model the chemistry in molecular clouds in the LMC and the SMC are interesting considering them from observations estimated high abundance of C_2H in the LMC and the SMC. Generally, when comparing with the observed abundances in N159W and N27, the Millar & Herbst model overestimates, whereas the Bel et al. model underestimates the abundances. An exception is CO, which abundance is reasonably well reproduced by the models. Also HCN, CN, and interestingly C_2H and CH_3OH early-time abundances in the Millar & Herbst model L2 agree fairly well with the observed ones in N159W. However, for CH_3OH the agreement may be a coincidence since its abundance has a strong time-dependence.

Recent models of the gas-phase chemistry in dense PDRs (with Galactic metallicity) developed by Fuente et al. (1993), Jansen et al. (1995a) and Bergin et al. (1997b) show that C_2H peaks at a rather low visual extinction, i.e. in the same region where molecular ions and C^+ are common. Simple hydrocarbons (CH_x, x=1–3) peak near the cloud boundary in the Sternberg & Dalgarno (1995) model as well; unfortunately they did not present results for C_2H.

Furthermore, in the models by Sternberg & Dalgarno (1995) and Jansen et al. (1995a) e.g. H_2O together with molecular ions like HCO^+ and SO^+ tend to have two peaks in their abundance distributions; one near the cloud boundary (i.e. at low A_V) – where also C^+, CO^+ and OH are abundant – reflecting the importance of photon-driven chemistry and emphasizing the formation routes of HCO^+ involving C^+; and a second one deep in the cloud interior where dark cloud chemistry, driven by cosmic-ray ionisation, dominates. This is in contrast to the behaviour of molecules such as CS and SO, whose abundances peak in the interior of the cloud.

Observations show that the abundances of C_2H and HCO^+ appear to be high in some diffuse clouds in the Galaxy (Liszt 1995; Liszt & Lucas 1994; Lucas & Liszt 1993, 1994, 1996; Hogerheijde et al. 1995), although Gredel et al. (1994) did not detect C_2H in their sample of translucent clouds. Also, Galactic translucent clouds and more dense PDRs show much higher H_2S abundances than can be obtained from present day chemical models of interstellar clouds (Tieftrunk et al. 1994; Jansen et al. 1995a). Thus, the observed abundances of C_2H and H_2S in the Magellanic Clouds, and the spatial distribution of HCO^+, can be qualitatively explained as results of a PDR-type chemistry. This requires that large volumes of the molecular ISM in star-forming regions in the Magellanic Clouds are 'translucent' for FUV photons, e.g. due to a high degree of clumpiness as is indicated by our data (cf. Sect. 5.1.2).

6. Conclusions

In this study we have, based on observations of molecular line emission at mm–wavelengths, compared the physical conditions and the molecular abundances in a small sample of interstellar molecular clouds in the Magellanic Clouds (N159S, N159W, N160, 30Dor-10, and 30Dor-27 in the LMC, and N27 in the SMC). Moreover, the HCO^+(J=1–0) line has been observed in four additional sources in the SMC. Relative to Galactic molecular clouds, the molecular clouds [with the cloud boundary defined by the CO(J=1–0) line emission] in the LMC and the SMC are found to be more clumpy, and to have lower abundances of trace molecules. The observed abundances of C_2H and H_2S, the abundance variation of C_2H and HCO^+, and the distribution of HCO^+ suggest that the chemical nature of molecular clouds in the LMC and the SMC is best described by PDR-type models.

More quantitatively, our main results are as follows:

1. A search for selected molecular species in the cloud associated with the H II region N27 in the SMC resulted in the detection of line emission from CO, ^{13}CO, CS, HCO^+, $H^{13}CO^+$ (marginal detection), SO, HCN, C_2H, and H_2CO. In addition, we report on detections of ortho-H_2S (first detection in an extragalactic source), CH_3OH (thermal emission), CH_3CCH, and, tentatively, H_2CS in N159W in the LMC.
2. The kinetic temperature and the number density of molecular hydrogen in N159W are estimated to be 25 ± 10 K and $(1\text{–}10)\times10^5$ cm^{-3}, respectively. CO lines give density estimates in the range a few$\times10^3$–1×10^6 cm^{-3}. The corresponding numbers for N27 are 15 ± 5 K and $(5\text{–}50)\times10^4$ cm^{-3}. Hence, the metallicity difference between the LMC and the SMC does not seem to affect the physical state of the gas dramatically.
3. Of the trace molecules detected so far in the Magellanic Clouds, C_2H appears to be the most abundant next to the CO isotopomers. The average abundance of C_2H in seven clouds in the LMC is 5×10^{-9}, which is similar to the abundance in Galactic star-forming clouds. In the SMC, the average C_2H abundance in two clouds is 3×10^{-9}.
4. Provided that the hydrogen is mainly in molecular form, the molecular abundances inside the region defined by CO line emission are typically five to twenty times lower in N159W than in Galactic clouds. Since the metallicity in H II regions in the Galaxy and the LMC differs only by a factor of $\approx$3, a combination of a lower metallicity and higher photodissociation rates of molecules in N159W is needed to explain the lower abundances.
5. The molecular abundances in the 30Dor-10 cloud located in the centre of the 30Dor region are on the average eight times lower than in N159W. We suggest that this underabundance is mainly caused by a more rapid photodissociation due to the more intense FUV radiation in 30Dor. The abundance deficit correlates well with the higher Hα and FUV fluxes in the central part of the 30Dor area.
6. The molecular abundances in N27 are on the average six times lower than in N159W. We attribute this underabundance to the lower metallicity in the SMC.
7. An alternative explanation to the underabundances of trace molecules in both 30Dor-10 and N27 would be a higher H/H_2 ratio inside these clouds as compared to the rest of the sample. In 30Dor-10 this could result from a more rapid photodissociation of H_2 due to the high FUV flux, while in N27 the cause could be a combination of a lower formation rate and a more rapid photodissociation of H_2 due to the lower dust abundance.
8. The CO(J=1–0)/HCO^+(J=1–0) line intensity ratio shows the same trend in the SMC as in the LMC, viz. a decreasing ratio with an increasing star-formation activity. The same trend is also exhibited by the CO(J=1–0)/C_2H(N=1–0) line intensity ratio in the LMC.
9. Using HCO^+ and $H^{13}CO^+$ data we estimated the gas-phase ^{12}C/^{13}C abundance ratio to be 40–90 in N27, and 35 ± 21 in 30Dor-10. Within the large uncertainties, these values are similar to the ratio estimated for N159W and Galactic disc clouds. However, the general trend in the LMC may be that the ^{12}C/^{13}C ratio is somewhat lower there than in Galactic disc clouds. More generally, our data do not support the notion that low-metallicity gas is poor in ^{13}C leading to a high ^{12}C/^{13}C ratio.

Acknowledgements. We thank S.J. Curran and the SEST staff for observing some of the spectral lines presented here. The line emission maps were analysed with the XSpec data-reduction software developed by P. Bergman.

Appendix A: LTE formulae

Here we list the expressions used in the calculation of the molecular column densities in the LTE approximation.

Assuming optically thin line emission and accounting for the background continuum radiation, the column density [N in cm^{-2}] of molecules populating the energy levels according to the Boltzmann distribution can be written:

$$N = \frac{1.67\times10^{14}\ \exp\left(E_{\rm upper}/{\rm k_B}T_{\rm ex}\right) Q(T_{\rm ex})\, I_0}{\left(1-\frac{F(T_{\rm bg})}{F(T_{\rm ex})}\right)\,\nu\,\mu_{\rm el}^2\,S\,g_{IK}} \qquad \text{(A1)}$$

where

$$F(T) = \frac{1}{\exp\left(\mathrm{h}\nu/\mathrm{k_B}T\right) - 1} \tag{A2}$$

$T_{\rm ex}$ [K] is the excitation temperature of the line, $T_{\rm bg}$ [K] is the temperature of the background radiation, ν [GHz] is the line frequency, $\mu_{\rm el}$ [Debye] is the electric dipole moment, S is the line-strength, g_{IK} is the statistical weight due to possible nuclear spin and K-degeneracy, Q is the partition function, and I_0 [K km s^{-1}] is the integrated intensity of the line. In cases when several transitions of a molecule have been observed, both the excitation temperature and the column density can be estimated (e.g. Turner 1991). This is straight-forward if the term involving the background radiation [$F(T_{\rm bg})$] is set to zero. We have followed this procedure and determined the excitation temperature from a multi-level analysis, and corrected for the background radiation a posteriori. The presented column densities (Table 17) are averages of the column densities, corrected for the background radiation, obtained from the various observed transitions. In cases where we lack multi-level data, we have assumed an excitation temperature close to that of a species with similar excitation requirements.

For linear rotors ($^1\Sigma$) we used the following partition function:

$$Q = \frac{\mathrm{k_B}T_{\rm ex}}{\mathrm{h}B} + \frac{1}{3} \tag{A3}$$

where B is the rotation constant.

For SO we made a direct summation over the energy levels with $E_{\rm n}/\mathrm{k_B} < 550$ K:

$$Q = \sum g_n \ (2J+1) \exp\left(-E_{\rm n}/\mathrm{k_B}T\right) \tag{A4}$$

g_n is the statistical weight of the energy level n: $g_n = 1$ for the ground state and $g_n = 3$ for all other states.

For H_2S we used:

$$Q = 2 \times \sqrt{\frac{\pi \mathrm{k_B}^3 T_{\rm ex}^3}{\mathrm{h}^3 ABC}} \approx 0.0977 \times T_{\rm ex}^{3/2} \tag{A5}$$

where A, B, and C are the rotation constants: A=310 583.57 MHz, B=270 367.68 MHz, and C=141 820.03 MHz. The contributions from both the ortho-species and the para-species have been accounted for.

For CH_3OH we used:

$$Q = 2 \times \sqrt{\frac{\pi \mathrm{k_B}^3 T_{\rm ex}^3}{\mathrm{h}^3 ABC}} \approx 1.233 \times T_{\rm ex}^{3/2} \tag{A6}$$

with A=127 511.6 MHz, B=24 687.04 MHz, and C=23 762.76 MHz. The contributions from both the A-symmetry species and the E-symmetry species have been accounted for. The contribution from each symmetry species is identical.

For CH_3CCH we used:

$$Q = \frac{8}{3} \times \sqrt{\frac{\pi \mathrm{k_B}^3 T_{\rm ex}^3}{\mathrm{h}^3 ABC}} \approx 4.177 \times T_{\rm ex}^{3/2} \tag{A7}$$

with A=158 590.0 MHz, and B=C=8 545.86 MHz.

For H_2CO, we calculated an analytical approximation for the partition function separately for the ortho and the para species. Each individual K-ladder was treated as a rigid symmetric top. The energy ($E_{J,K}$) of a state described by the quantum numbers J and K, was split into a part describing the ground-state energy of the K-ladder in question and a J dependent part:

$$\begin{aligned} E_{J,K} \ = \ & \mathrm{h}\left(B\,K\,(K+1) + (A-B)\,K^2\right) + \\ & \mathrm{h}B\left(J\,(J+1) - K\,(K+1)\right) \end{aligned} \tag{A8}$$

Approximating the partition function for an individual K-ladder with an integral and adding the partition functions for the two lowest K-ladders for each of the ortho and para species separately, we arrive at the following expressions:

$$Q_{\rm para} = Q_{K=0} + Q_{K=2} \tag{A9}$$

$$Q_{\rm ortho} = Q_{K=1} + Q_{K=3} \tag{A10}$$

with

$$Q_{K=0} = 0.5721 \times T_J + \frac{1}{3} \tag{A11}$$

$$Q_{K=1} = 6 \times \left(0.5721 \times T_J - \frac{2}{3}\right) \tag{A12}$$

$$\begin{aligned} Q_{K=2} = \ & 2 \times \exp\left(-47.13/T_K\right) \times \\ & \left(0.5721 \times T_J - \frac{2}{3} - 3 \times \exp\left(-3.50/T_J\right)\right) \end{aligned} \tag{A13}$$

$$\begin{aligned} Q_{K=3} = \ & 6 \times \exp\left(-94.90/T_K\right) \times \\ & \left(0.5721 \times T_J - \frac{2}{3} - 3 \times \exp\left(-3.50/T_J\right)\right. \\ & \left. -5 \times \exp\left(-10.49/T_J\right)\right) \end{aligned} \tag{A14}$$

T_J is the excitation temperature between two K-ladders (i.e. J fixed and K varies) and T_K the excitation temperature along a fix K-ladder (i.e. K fixed and J varies). This allows to take into account the fact that the excitation along a K-ladder differs form the excitation across different K-ladder because fast radiative transitions are allowed in the former case but forbidden in the latter case. T_K is likely to be a good indicator of the kinetic temperature (see also Mangum & Wootten 1993). The energies for the ortho-species are here calculated relative to a 'virtual' ground-state, lying 11.67 K above the para ground-state. With a 'virtual' ground-state we mean, that the lowest energy is thought of as that of the J=0, K=0 state which does not exist for ortho-H_2CO. Its 'true' ground-state, with an energy of 15.16 K above the para ground-state, is J=1, K=1.

References

Avery L.W., Green S., 1989, ApJ 337, 306
Bachiller R., Fuente A., Bujarrabal, et al., 1997, A&A 319, 235
Batchelor R.A., McCulloch M.G., Whiteoak J.B., 1981, MNRAS 194, 911

Beasley A.J., Ellingsen S.P., Claussen M.J., Wilcots E., 1996, ApJ 459, 600
Bel N., Viala Y.P., Guidi I., 1986, A&A 160, 301
Bergin E.A., Ungerechts H., Goldsmith P.F., et al., 1997a, ApJ 482, 267
Bergin E.A., Goldsmith P.F., Snell R.L., Langer W.D., 1997b, ApJ 482, 285
Black J.H., 1987, In: Hollenbach D.J., Thronson H.A. (eds.) Interstellar Processes. Reidel, Dordrecht, p. 731
Blake G.A., Sutton E.C., Masson C.R., Phillips T.G., 1987, ApJ 315, 621
Bohlin R.C., Savage B.D., Drake J.F., 1978, ApJ 224, 132
Boreiko R.T., Betz A.L., 1991, ApJ 380, L27
Bouchet P., Lequeux J., Maurice E., Prévot L., Prévot-Burnichon M.L., 1985, A&A 149, 330
Caldwell D.A., 1997, Ph.D. Thesis, Rensselaer Polytechnic Institute, Troy, New York
Caplan J., Deharveng L., 1985, A&AS 62, 63
Caplan J., Deharveng L., 1986, A&A 155, 297
Caplan J., Taisheng Ye., Deharveng L., Turtle A.J., Kennicutt R.C., 1996, A&A 307, 403
Caswell J.L., Haynes R.F., 1981, MNRAS 194, 33P
Charnley S.B., 1997, ApJ 481, 396
Charnley S.B., Tielens A.G.G.M., Millar T.J., 1992, ApJ 399, L71
Chin Y.-N., Henkel C., Whiteoak J.B., Langer N., Churchwell E.B., 1996a, A&A 305, 960
Chin Y.-N., Henkel C., Millar T.J., Whiteoak J.B., Mauersberger R., 1996b, A&A 312, L33
Chin Y.-N., Henkel C., Whiteoak J.B., et al., 1997, A&A 317, 548
Chin Y.-N., Henkel C., Millar T.J., Whiteoak J.B., Marx-Zimmer M., 1998, A&A 330, 901
Cohen R.S., Dame T.M., Garay G., et al., 1988, ApJ 331, L95
Dahmen G., Wilson T.L., Matteucci F., 1995, A&A 295, 194
Dennefeld M., 1989, In: de Boer K.S., Spite F., Stasinska G. (eds.) Recent Developments of Magellanic Clouds Research. Observatoire de Paris, p. 107
Ellingsen S.P., Whiteoak J.B., Norris R.P., Caswell J.L., Vaile R.A., 1994, MNRAS 269, 1019
Feast M.W., 1995, In: van der Kruit P.C., Gilmore G. (eds.) Proc. IAU Symp. 164, Stellar Populations. Kluwer, Dordrecht, p. 153
Friberg P., Madden S.C., Hjalmarson Å., Irvine W.M., 1987, A&A 195, 281
Fuente A., Martín-Pintado J., Cernicharo J., Bachiller R., 1993, A&A 276, 473
Garnett D.R., Skillman E.D., Dufour R.J., et al., 1995, ApJ 443, 64
Gottlieb C.A., Gottlieb E.W., Litvak M.M., Ball J.A., Penfield H., 1978, ApJ 219, 77
Gredel R., van Dishoeck E.F., Black J.H., 1994, A&A 285, 300
Heikkilä A., 1996, Licentiate thesis, Chalmers University of Technology, Göteborg
Heikkilä A., 1998, Ph.D. thesis, Chalmers University of Technology, Göteborg
Heikkilä A., Johansson L.E.B., Olofsson H., 1997a, A&A 319, L21
Heikkilä A., Johansson L.E.B., Olofsson H., 1997b, In: Jansen D.J., Hogerheijde M.R., van Dishoeck E.F. (eds.) IAU symposium 178 Abstract Book, Molecules in Astrophysics Probes & Processes. Sterrewacht Leiden, p. 301
Heikkilä A., Johansson L.E.B., Olofsson H., 1998, A&A 332, 493
Helmich F.P., van Dishoeck E.F., 1997, A&AS 124, 205
Henkel C., Mauersberger R., Wiklind T., et al., 1993, A&A 268, L17
Henkel C., Whiteoak J.B., Mauersberger R., 1994, A&A 284, 17
Henkel C., Chin Y.-N., Mauersberger R., Whiteoak J.B., 1998, A&A 329, 443
Hogerheijde M.R., de Geus E.J., Spaans M., van Langevelde H.J., van Dishoeck E.F., 1995, ApJ 441, L93
Holtzman J.A., Mould J.R., Gallagher J.S., et al., 1997, AJ 113, 656
Huggins P.J., Gillespie A.R., Phillips T.G., Gardner F., Knowles S., 1975, MNRAS 173, 69P
Israel F.P., de Graauw T., Lidholm S., van de Stadt H., de Vries C., 1982, ApJ 262, 100
Israel F.P., de Graauw Th., van de Stadt H., de Vries C.P., 1986, ApJ 303, 186
Israel F.P., Koornneef J., 1988, A&A 190, 21
Israel F.P., Maloney P.R., 1993, In: Baschek B., Klare G., Lequeux J. (eds.) New Aspects of Magellanic Cloud Research. Springer-Verlag, Berlin, p. 44
Israel F.P., Johansson L.E.B., Lequeux J., et al., 1993, A&A 276, 25
Israel F.P., Maloney P.R., Geis N., et al., 1996, ApJ 465, 738
Jansen D.J., van Dishoeck E.F., Black J.H., 1994, A&A 282, 605
Jansen D.J., van Dishoeck E.F., Black J.H., Spaans M., Sosin C., 1995a, A&A 302, 223
Jansen D.J., Spaans M., Hogerheijde M.R., van Dishoeck E.F., 1995b, A&A 303, 541
Johansson L.E.B., Andersson C., Elldér J., et al., 1984, A&A 130, 227
Johansson L.E.B., 1991, In: Combes F., Casoli F. (eds.) Proc. IAU Symp. 146, Dynamics of Galaxies and Their Molecular Cloud Distributions. Kluwer, Dordrecht, p. 1
Johansson L.E.B., 1997, In: van Dishoeck E.F. (ed.) Proc. IAU Symp. 178, Molecules in Astrophysics: Probes & Processes. Kluwer, Dordrecht, p. 515
Johansson L.E.B., Olofsson H., Hjalmarson Å., Gredel R., Black J.H., 1994, A&A 291, 89 (Paper I)
Johansson L.E.B., Greve A., Booth R.S., et al., 1998, A&A 331, 857
Koornneef J., 1982, A&A 107, 247
Koornneef J., Israel F.P., 1985, ApJ 291, 156
Kutner M.L., Rubio M., Booth R.S., et al., 1997, A&AS 122, 255
Langer W.D., Graedel T.E., Frerking M.A., Armentrout P.B., 1984, ApJ 277, 581
Lequeux J., 1989, In: de Boer K.S., Spite F., Stasinska G. (eds.) Recent Developments of Magellanic Clouds Research. Observatoire de Paris, p. 119
Lequeux J., Le Bourlot J., Pineau des Forêts G., et al., 1994, A&A 292, 371
Liszt H.S., 1995, ApJ 442, 163
Liszt H.S., Lucas R., 1994, ApJ 431, L131
Liszt H.S., Lucas R., 1998, A&A 339, 561
Lovas F.J., 1992, J. Phys. Chem. Ref. Data 21, 181
Lucas R., Liszt H.S., 1993, A&A 276, L33
Lucas R., Liszt H.S., 1994, A&A 282, L5
Lucas R., Liszt H.S., 1996, A&A 307, 237
MacLaren I., Richardson K.M., Wolfendale A.W., 1988, ApJ 333, 821
Maloney P., Black J.H., 1988, ApJ 325, 389
Mangum J.G., Wootten A., 1993, ApJS 89, 123
Menten K.M., Walmsley C.M., Henkel C., Wilson T.L., 1988, A&A 198, 253
Millar T.J., 1997, In: van Dishoeck E.F. (ed.) Proc. IAU Symp. 178, Molecules in Astrophysics: Probes & Processes. Kluwer, Dordrecht, p. 75
Millar T.J., Bennett A., Herbst E., 1989, ApJ 340, 906
Millar T.J., Herbst E., 1990, MNRAS 242, 92
Millar T.J., Farquhar P.R.A., Willacy K., 1997, A&AS 121, 139
Minh Y.C., Ziurys L.M., Irvine W.M., McGonagle D., 1990, ApJ 360, 136

Minh Y.C., Ziurys L.M., Irvine W.M., McGonagle D., 1991, ApJ 366, 192
Mitchell G.F., 1984, ApJS 54, 81
Mitchell G.F., Ginsburg J.L., Kuntz P.J., 1978, ApJS 38, 39
Mochizuki K, Nakagawa T., Doi Y., et al., 1994, ApJ 430, L37
Nummelin A., Bergman P., Hjalmarson Å., et al. 1998, ApJS 117, 427
Ohishi M., Irvine W.M., Kaifu N., 1992, In: Singh P. (ed.) Proc. IAU Symp. 150, Astrochemistry of Cosmic Phenomena. Kluwer, Dordrecht, p. 171
Olofsson H., Eriksson K., Gustafsson B., Carlström U., 1993, ApJS 87, 305
Olofsson H., Bergman P., Eriksson K., Gustafsson B., 1996, A&A 311, 587
Pak S., Jaffe D.T., van Dishoeck E.F., Johansson L.E.B., Booth R.S., 1998, ApJ 498, 735
Peimbert M., Torres-Peimbert S., Dufour R.J., 1993, ApJ 418, 760
Poglitsch A., Krabbe A., Madden S.C., et al., 1995, ApJ 454, 293
Rodrigues C.V., Magalhães A.M., Coyne G.V., Piirola V., 1997, ApJ 485, 618
Rodríguez-Franco A., Martín-Pintado J., Fuente A., 1998, A&A 329, 1097
Rubio M., Garay G., Montani J., Thaddeus P., 1991, ApJ 368, 173
Rubio M., Lequeux J., Boulanger F., et al., 1993, A&A 271, 1
Rubio M., Lequeux J., Boulanger F., et al., 1996, A&AS 118, 263
Scalise E., Braz M.A., 1982, AJ 87, 528
Schilke P., Walmsley C.M., Pineau des Forêts G., et al., 1992, A&A 256, 595
Schwering P., 1988, Ph.D. thesis, University of Leiden
Schwering P.B.W., Israel F.P., 1989, A&AS 79, 79
Sinclair M.W., Carrad G.J., Caswell J.L., Norris R.P., Whiteoak J.B., 1992, MNRAS 256, 33P
Skatrud D.D., De Lucia F., Blake G.A., Sastry K.V.L.N., 1983, J. Mol. Spec. 99, 35
Solomon P.M., Rivolo A.R., Barrett J., Yahil A., 1987, ApJ 319, 730
Stappers B.W., Mould J.R., Sebo K.M., et al., 1997, PASP 109, 292
Sternberg A., Dalgarno A., 1995, ApJS 99, 565
Tieftrunk A., Pineau des Forêts G., Schilke P., Walmsley C.M., 1994 A&A 289, 579
Tielens A.G.G.M., Allamandola L.J., 1987, In: Hollenbach D.J., Thronson H.A. (eds.) Interstellar Processes. Reidel, Dordrecht, p. 397
Tucker K.D., Kutner M.L., Thaddeus P., 1974, ApJ 193, L115
Turner B.E., 1991, ApJS 76, 617
Turner B.E., 1996, ApJ 468, 721
Turner B.E., Pirogov L., Minh Y.C., 1997, ApJ 483, 235
Turner B.E., Lee H.-H., Herbst E., 1998, ApJS 115, 91
Ungerechts H., Bergin E.A., Goldsmith P.F., et al., 1997, ApJ 482, 245
van der Werf P.P., Stutzki J., Sternberg A., Krabbe A., 1996, A&A 313, 633
Vrtilek J.M., Gottlieb C.A., Thaddeus P., 1987, ApJ 314, 716
Watson W.D., 1972, ApJ 176, 103
Werner M.W., Becklin E.E., Gatley I., et al., 1978, MNRAS 184, 365
Westerlund B.E., 1990, A&AR 2, 29
Westerlund B.E., 1997, The Magellanic Clouds. Cambridge Univ. Press, Cambridge
Westerlund B.E., Danzinger I.J., 1985, In: Shaver P.A., Kjär K. (eds.) Proc. ESO-IRAM-Onsala Workshop on (Sub)Millimeter Astronomy. European Southern Observatory, p. 207
Whiteoak J.B., Gardner F.F., 1976a, MNRAS 174, 51P
Whiteoak J.B., Gardner F.F., 1976b, MNRAS 176, 25P
Whiteoak J.B., Gardner F.F., Höglund B., 1980, MNRAS 190, 17P
Whittet D.C.B., Schutte W.A., Tielens A.G.G.M., et al., 1996, A&A 315, L357
Wilson C.D., Walker C.D., Thornley M.D., 1997, ApJ 483, 210
Wilson T.L., Matteucci F., 1992, A&AR 4, 1
Wilson T.L., Rood R.T., 1994, ARA&A 32, 191
Wouterloot J.G.A., Brand J., 1996, A&AS 119, 439